HHS Public Access

Author manuscript

Circ Res. Author manuscript; available in PMC 2023 May 27.

Published in final edited form as:

Circ Res. 2022 May 27; 130(11): 1662–1681. doi:10.1161/CIRCRESAHA.121.320420.

Perivascular Fibrosis Is Mediated by a KLF10-IL-9 Signaling Axis in CD4+ T Cells

Rulin Zhuang[1,2,*], **Jingshu Chen**[1,*], **Henry S. Cheng**[1,*], **Carmel Assa**[1], **Anurag Jamaiyar**[1], **Arvind K. Pandey**[1], **Daniel Pérez-Cremades**[1,3], **Bofang Zhang**[1], **Aspasia Tzani**[1], **Akm Khyrul Wara**[1], **Jorge Plutzky**[1], **Victor Barrera**[4], **Preetida Bhetariya**[4], **Richard N. Mitchell**[5], **Zhongmin Liu**[2], **Mark W. Feinberg**[1,#]

[1]Department of Medicine, Cardiovascular Division, Brigham and Women's Hospital, Harvard Medical School, Boston, MA 02115, USA

[2]Department of Cardiovascular Surgery, Shanghai East Hospital, Tongji University School of Medicine, Shanghai, 200120, China

[3]Department of Physiology, University of Valencia, and INCLIVA Biomedical Research Institute, Valencia 46010, Spain.

[4]Department of Biostatistics, Harvard T.H. Chan School of Public Health, Boston, MA 02115, USA

[5]Department of Pathology, Brigham and Women's Hospital, Harvard Medical School, Boston, MA 02115, USA

Abstract

Background: Perivascular fibrosis, characterized by increased amount of connective tissue around vessels, is a hallmark for vascular disease. Angiotensin II (Ang II) contributes to vascular disease and end-organ damage via promoting T-cell activation. Despite recent data suggesting the role of T cells in the progression of perivascular fibrosis, the underlying mechanisms are poorly understood.

Methods: Transcription factor profiling was performed in peripheral blood mononuclear cells of hypertensive patients. CD4-targeted KLF10 deficient ($Klf10^{fl/fl}CD4^{Cre+}$; (TKO)) and CD4-Cre ($Klf10^{+/+}CD4^{Cre+}$; (Cre)) control mice were subjected to Ang II infusion. Endpoint characterization included cardiac echocardiography, aortic imaging, multi-organ histology, flow cytometry, cytokine analysis, aorta and fibroblast transcriptomic analysis, and aortic single-cell RNA-sequencing (scRNA-seq).

Results: Transcription factor profiling identified increased *KLF10* expression in hypertensive human subjects and in CD4+ T cells in Ang II treated mice. TKO mice showed enhanced perivascular fibrosis, but not interstitial fibrosis, in aorta, heart, and kidney in response to Ang

[#]To whom correspondence should be addressed: Mark W. Feinberg, M.D. Department of Medicine, Cardiovascular Division, Brigham and Women's Hospital, Harvard Medical School, Boston, MA 02115, USA. Fax: 617-525-4380. Tel: 617-525-4381. mfeinberg@bwh.harvard.edu.

[*]These authors contributed equally to this work.

Disclosures section

The authors have declared that no competing interests exist.

II, accompanied by alterations in global longitudinal strain, arterial stiffness, and kidney function compared to Cre control mice. However, blood pressure was unchanged between the two groups. Mechanistically, KLF10 bound to the IL-9 promoter and interacted with HDAC1 to inhibit IL-9 transcription. Increased IL-9 in TKO mice induced fibroblast intracellular calcium mobilization, fibroblast activation and differentiation, and increased production of collagen and extracellular matrix, thereby promoting the progression of perivascular fibrosis and impairing target organ function. Remarkably, injection of anti-IL9 antibodies reversed perivascular fibrosis in Ang II-infused TKO mice and C57BL/6 mice. scRNA-seq revealed fibroblast heterogeneity with activated signatures associated with robust ECM and perivascular fibrosis in Ang II-treated TKO mice.

Conclusions: CD4+ T cell deficiency of *Klf10* exacerbated perivascular fibrosis and multi-organ dysfunction in response to Ang II via upregulation of IL-9. *Klf10* or IL-9 in T cells might represent novel therapeutic targets for treatment of vascular or fibrotic diseases.

Graphical Abstract

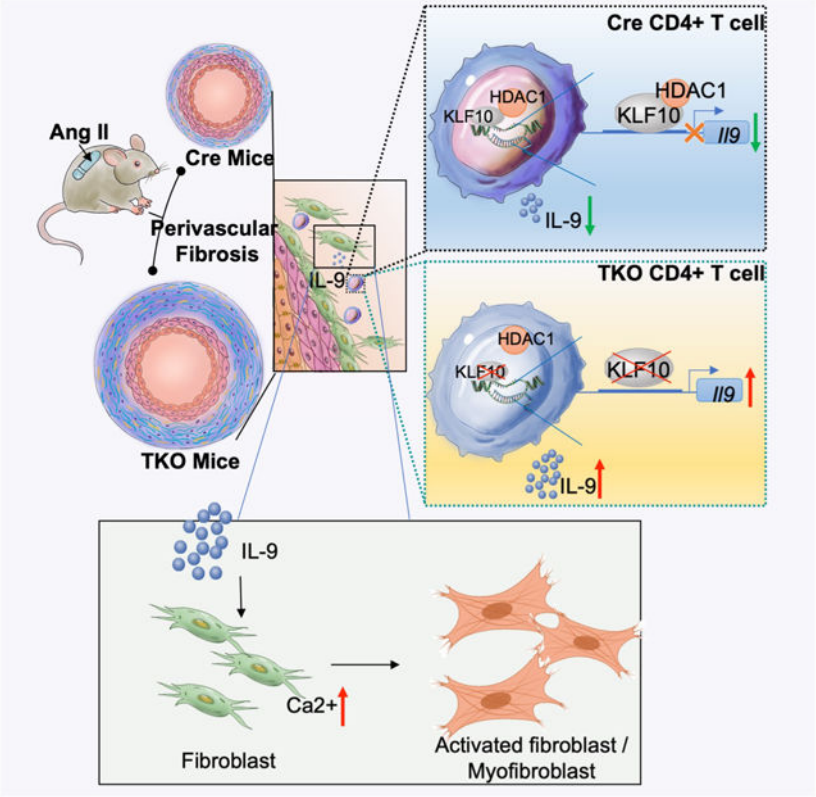

Keywords

Animal Models of Human Disease; Fibrosis; Growth Factors/Cytokines; Vascular Biology Basic Science Research

Introduction

Perivascular fibrosis is a hallmark of advanced vascular disease states often associated with elevated blood pressure, vascular stiffness, adverse vascular remodeling, and end-organ dysfunction such as in the heart and kidney.[1, 2] Continuous excessive stress and inflammation during hypertension increase the amount of perivascular connective tissue and collagen deposition that is characteristic of pathological perivascular fibrosis.[3] Indeed, hypertension remains a serious public health problem that contributes to considerable global cardiovascular disease and premature death worldwide[4] by increasing the risk of ischemic heart disease, stroke, and chronic kidney disease.[5] Early management and therapeutic intervention may greatly reduce the occurrence or postpone the development of chronic fibrotic diseases, especially hypertensive cardiovascular, kidney, and aortic disease. However, therapeutic targets that specifically control perivascular fibrosis are not well defined.

Accumulating studies revealed that perivascular fibrosis is greatly dependent on perivascular inflammation and immune cells in hypertension.[6-9] Angiotensin II (Ang II) contributes to vascular damage and end-organ damage via promoting T-cell activation and proliferation.[10] The importance of T cells in the progression of perivascular fibrosis has been highlighted recently through the prevention of aortic fibrosis and stiffening in *Rag1−/−* mice, which was reversed by adoptive transfer of T cells after Ang II infusion.[6]Furthermore, Ang II induced T cell-derived microRNA-214 mediated perivascular fibrosis, vascular stiffening, and dysfunction by regulating T cell activation and chemotaxis in hypertension.[11] Despite recent data suggesting the role of T cells in the progression of perivascular fibrosis, the underlying mechanisms remain poorly understood.

Kruppel-like Factor 10 (KLF10), a transcription factor that belongs to the kruppel-like zinc-finger family, was found to be expressed in T cell subsets. Our previous studies demonstrated that KLF10 regulates both CD4+CD25− T cell effectors and CD4+CD25+ regulatory T cells thereby regulating atherosclerotic lesion formation in a murine atherosclerosis model [12]. Furthermore, we also found that KLF10 in CD4+ T cells regulate obesity, insulin resistance, and fatty liver in the presence of a high fat diet.[13] Given the prominent role of CD4+ T cells in mediating a range of Ang II-associated vascular diseases, we hypothesized that KLF10 in CD4+ T cells may contribute to the regulation of vascular remodeling. Herein, we find that CD4-targeted KLF10 deficient (TKO) mice develop marked acceleration of perivascular fibrosis, but not interstitial fibrosis, through distinct mechanisms involving CD4+ T cell release of IL-9 and activation of specific fibroblast and myofibroblast subsets.

Methods

Data Availability

The data, methods used in the analysis, and materials used to conduct the research of this study are available from the corresponding author upon reasonable request. Major Resources Table, detailed methods, and supplementary figures are provided in the Supplementary Material.

Results

KLF10 expression is increased in CD4+ T cells after Ang II treatment

Given the importance of transcriptional control of leukocytes in hypertension[14-18], dysregulated transcription factors (TFs) were examined from a published dataset of hypertensive patients with or without left ventricular (LV) remodeling in peripheral blood mononuclear cells (PBMCs). Multiple TFs were found dysregulated in hypertensive patients with or without LV remodeling compared with control individuals (Figure 1A). However, only two TFs (*KLF10* and *STAT3*) were found commonly dysregulated in hypertensive patients with or without LV remodeling compared to controls (Figure 1B). The increased expression of *KLF10* was further confirmed in an independent dataset of uncontrolled hypertensive subjects (Figure 1C). Considering the important regulatory role of KLF10 in CD4+ T cells in atherosclerosis,[12] obesity and insulin resistance[13], we sought to investigate if *Klf10* expression was altered in T cells in a murine model of hypertension. RNA-sequencing from Ang II-treated mice revealed *Klf10* to be one of the top TFs significantly increased in splenic CD3+ T cells (Figure 1D). This was confirmed by RT-qPCR analysis of isolated CD3− cells, CD3+, and CD4+ T cells from the spleen after 28 days of Ang II treatment in which *Klf10* expression increased in response to Ang II in CD3+ T cells and even higher in CD4+ T cells (Figure 1E). Because Ang II treatment is known to impact vascular remodeling[19], co-staining of KLF10 and CD4+ T cells was performed in cross-sections of the descending aorta. Higher counts of CD4+KLF10+ cells were observed after Ang II treatment compared with the PBS infused group (Figure 1F). To identify whether Ang II can increase *Klf10* in T cells, CD4+ T cells were isolated from C57BL/6 mice and treated with increasing amounts of Ang II. *Klf10* expression was found to be significantly up-regulated by Ang II in a dose-dependent manner (Figure 1G). Taken together, KLF10 expression increased in PBMCs in hypertensive patients, and in CD4+T cells after Ang II treatment in mice, highlighting a potential role of *Klf10* in CD4+T cell in Ang II-induced vascular remodeling.

KLF10 deficiency in CD4+ T cells impairs the function of hypertension-related organs and triggers perivascular fibrosis independent of blood pressure

To evaluate the role of KLF10 in CD4+ T cells in Ang II-induced vascular remodeling, CD4-targeted KLF10 deficient ($Klf10^{fl/fl}CD4^{Cre+}$, (TKO)) and CD4-Cre ($Klf10^{+/+}CD4^{Cre+}$, (Cre)) control mice[13] were infused with PBS or Ang II for 28 or 42 days (Figure 2A). Aortic blood pressure increased in the Ang II treatment groups compared to PBS controls; however, no difference was found between TKO and Cre control mice in both 28 days and 42 days (Figure 2B). Considering Ang II-induced hypertension can cause tissue remodeling and multi-organ dysfunction, we further evaluated the function of heart, aorta, and kidney in these mice. After 28 days of Ang II infusion, hearts of TKO mice demonstrated impaired LV global longitudinal strain (GLS, Figure 2C, Table S3); furthermore, aortas of TKO mice developed increased abdominal pulse-wave velocity (PWV, Figure 2D) and decreased circumferential strain (Circ Strain, Figure 2E) compared to Cre control mice, while there were no differences prior to Ang II infusion (Figure S1A, B). Similarly, following 28 days of Ang II infusion, TKO mice demonstrated smooth muscle hypercontractility compared to Cre control mice, and both smooth muscle hypercontractility and impaired smooth muscle

relaxation manifested after 42 days of Ang II infusion (Figure S1C, D). Ang II infusion also resulted in a marked increase of albuminuria and kidney injury molecule-1 (KIM-1) levels as detected in the urine of TKO mice (Figure 2F, G), while no statistical difference was observed under basal conditions compared with control mice (Figure S1E, F). Altogether, our results suggest end organ dysfunction and likely tissue remodeling occurred after Ang II infusion in mice deficient of *Klf10* in CD4+ T cells, effects that were independent of blood pressure differences between TKO and Cre control mice.

As a cardiovascular damage inducer, chronic Ang II infusion can induce significant hypertension, cardiomyocyte hypertrophy, and fibrosis in mice[20, 21]. To identify histopathological changes, we first evaluated the hearts and found no histopathological difference in total fibrosis, interstitial fibrosis, and myocyte cross-sectional area between Cre and TKO groups after Ang II infusion (Figure S1G, H). However, perivascular fibrosis in the heart was markedly increased in TKO mice after Ang II treatment compared to Cre mice (Figure 2H). Similarly, increased perivascular fibrosis was also observed in the kidneys of TKO mice (Figure 2I). Furthermore, severe aortic perivascular fibrosis and adventitial collagen deposition were detected in Ang II treated TKO mice by Masson trichrome staining and Sirius red staining (Figure 2J and 2K). No differences in fibrosis or collagen were observed between TKO and Cre before Ang II treatment (Figure S1I). Analogous perivascular phenotypes were also found in female mice (Figure S1J). Collectively, our results indicate that mice deficient of *Klf10* in CD4+ T cells develop accelerated perivascular fibrosis compared to Cre control mice in aortas, hearts, and kidneys after Ang II infusion.

KLF10 deficient CD4+ T cells release IL-9 that mediates perivascular fibrosis

To elucidate possible mediators involved with the observed multi-organ perivascular fibrosis, we first examined the expression of angiotensin II receptors in CD4+T cells and fibroblasts; however, no differences were observed between the TKO and Cre control groups (Figure S2A and 2B). To identify potential mediators in the circulation, we performed plasma cytokine profiling from Ang II treated TKO and Cre mice (Figure S2C). Amongst a panel of inflammatory markers, IL-9 was the only significantly increased cytokine after Ang II treatment in both male and female TKO mice compared to controls (Figure 3A and S2D). In concordance, *Il9* expression was also upregulated in PBMCs, hearts, kidneys, and aortas (Figure 3B). Considering that Ang II treatment is known to increase the accumulation of leukocytes and T cells in tissues to mediate vascular dysfunction, hypertension, and end-organ inflammation[10, 22, 23], we sought to determine the role of CD4+IL9+ cells in vascular inflammation. Flow cytometry from single-cell suspensions of the thoracic aorta showed that the percentage of CD4+IL9+ cells and CD4+IL4+ cells increased in TKO mice after Ang II treatment, while no differences were observed in other cell types compared to Cre control including CD8+IL9+ cells (Figure 3C, S2E through S2G). Similar changes were found in the spleen (Figure 3D, S2H and S2I). Consistently, immunofluorescence imaging also captured the increase of CD4+IL9+ cells in the periadventitial tissue (Figure 3E, and S2J). Although the percentage of CD4+IL4+ T cells increased in TKO mice, there were no differences of released IL-13, IL-5, and IL-4 in both male and female TKO mice compared with Cre controls (Figure S2K and S2L). To confirm whether KLF10 deficiency in CD4+

T cells affected the production of IL-9, CD4+ T cells were isolated from Ang II-treated TKO and Cre mice (Figure 3F). CD4+ T cells from TKO mice had higher mRNA expression for *Il9* and released more IL-9 protein in supernatants compared to Cre controls (Figure 3G and S2M), while no differences were observed in secreted IL-5 and IL-4 (Figure S2N). Similarly, CD4+ T cells isolated from TKO or Cre mice and subsequently treated with Ang II *ex vivo* for 1 day (Figure 3H) demonstrated increased *Il9* expression and had a higher level of IL-9 protein release in supernatants from TKO CD4+ T cells compared to Cre CD4+ T cells (Figure 3I).

To further assess the role of IL-9 in the development of perivascular fibrosis, recombinant mIL9 was administrated in Ang II-treated Cre mice (Figure 3J). Systemic delivery of mIL9 markedly impaired LV GLS (Figure 3K, Table S4), increased PWV, and decreased Circ Strain (Figure 3L) in Cre mice. In addition, the ratio of albumin and creatinine, and the value of KIM-1 increased after treating with mIL9 (Figure 3M). Importantly, histopathological analyses confirmed that the mIL9 treated group developed severe perivascular fibrosis and increased adventitial collagen deposition (Figure 3N and 3O). Taken together, deficiency of *Klf10* in CD4+ T cells increased IL-9, and ectopic delivery of IL-9 mediated the perivascular fibrosis phenotype, effectively phenocopying the perivascular fibrosis observed in *Klf10*-deficient CD4+ T cell mice.

KLF10 binds to the IL-9 promoter and interacts with HDAC1 to inhibit IL-9 activation

Previous studies have demonstrated that KLF10 could bind to target gene promoters to regulate transcription.[24, 25] Given the increased expression of IL-9 in TKO mice and in TKO CD4+ T cells, we explored potential underlying mechanisms of this regulation. As shown in Figure 4A, there are four putative KLF10 DNA-binding sites in the *Il9* promoter sequence [26, 27]. Using chromatin immunoprecipitation assays with KLF10 antibodies in CD4+ T cells and the designated primer pairs directed for each putative binding site, we found that Ang II markedly increased the KLF10 enrichment to these sites (Figure 4B). Overexpression of mouse KLF10 by transfecting overexpression plasmid in a heterologous HEK293T cell was confirmed by Western blot (Figure 4C). It was shown that overexpression of mouse KLF10 in HEK293T cell significantly inhibited the transcriptional activity of a mouse IL9 promoter reporter (Figure 4D). In addition, 5’ truncations of the IL-9 promoter demonstrated that successive deletions of the putative KLF10 binding sites increased transcriptional activity of the IL-9 promoter, suggesting that KLF10 mediates transcriptional repression (Figure 4E). KLF10 has been reported to interact with histone deacetylase 1 (HDAC1) to facilitate transcriptional repression.[24, 25] Consistently, we found that KLF10 recruited HDAC1 in T cells, especially after Ang II treatment (Figure 4F). Next, we assessed the role of HDAC1 on IL-9 promoter in the presence of KLF10 by performing luciferase reporter assays (Figure 4G). Depletion of HDAC1 with siRNAs demonstrated elevated luciferase activity among the WT and 3 mutant IL-9 promoters (Figure 4G-H). Collectively, these findings suggest that KLF10 interacts with HDAC1 and binds to the proximal IL-9 promoter to inhibit IL-9 transcriptional activity.

Transcriptomic changes involved in Ang II-induced perivascular fibrosis

To ascertain the underlying global transcriptomic changes involved in perivascular fibrosis, we performed RNA-sequencing and gene ontology pathway analysis on stripped (perivascular adventitial tissue removed) (Figure S3) and non-stripped aorta (perivascular adventitial tissue remained intact) (Figure S4) from Cre or TKO mice after Ang II treatment. Comparison of stripped aortas between Cre and TKO mice revealed that most differentially regulated genes are related to metabolic processes but not to fibrotic process (Figure S3D through 3F). Considering the pathophysiological changes of fibrosis occurred in the perivascular adventitial tissue, we next focused our bioinformatic analysis on the non-stripped aortas. In contrast to Ang II-treated Cre mice, non-stripped aortas of TKO mice manifested pathways involved in assembly and muscle contraction ('Muscle contraction', 'Myofibril assembly'), ion transport, and sarcomere organization (Figure S4, 5A, S4E and S4F). To identify transcriptomic differences derived from the vessel and adventitial tissues, we compared overlapping and unique differentially expressed genes (DEGs) (FDR <0.05) from the stripped and non-stripped aortic TKO vs Cre contrasts (Figure 5B and S5). From a total of 48 overlapping DEGs between TKO and Cre aortas, gene set enrichment analyses revealed several pathways involved in fibrosis, junctional signaling, and ion-related pathways (Figure 5C). Notably, from the 748 unique DEGs derived from the non-stripped aorta, calcium signaling emerged as a dominant pathway in the TKO group (Figure 5D) and the significantly regulated calcium signaling pathway genes were shown in the heatmap (Figure 5E). As such, we performed von Kossa staining which revealed higher calcium deposition in the adventitial tissues from Ang II treated TKO mice compared to Cre controls (Figure 5F). Furthermore, calcium flux assays in isolated aortic fibroblasts (Figure S6A through S6D) from C57BL/6 mice were performed to detect the effect of IL-9 on intracellular calcium levels. Consistent with previous reports[28, 29], we found that Ang II as a pro-fibrotic agonist increased intracellular calcium; however, IL-9 further augmented this intracellular calcium flux in the presence of Ang II (Figure 5G, Video S1). Collectively, comparative RNA-seq transcript profiling identified several pathways associated with periadventitial remodeling and that the calcium signaling pathway is dominantly upregulated in non-stripped aortas of TKO mice after Ang II treatment. In addition, IL-9 and Ang II cooperatively increase calcium flux in aortic fibroblasts *ex vivo*.

TKO fibroblasts display an activation signature and IL-9 and Ang II treatment recapitulate the phenotype in control fibroblasts

Given that calcium is involved in particularly critical signaling pathways for fibroblast and myofibroblast differentiation[28, 30], we isolated and cultured aortic fibroblasts from Ang II-treated Cre control and TKO mice (Figure 6A). Immunofluorescence staining showed that the expression of Col1a1 and α-SMA increased significantly in aortic fibroblasts of TKO mice compared with those from Cre mice (Figure 6B, and S6A). RNA-sequencing of those TKO and Cre fibroblasts revealed upregulation of myofibroblast marker related genes (*Cnn1*, *Acta2*, etc.) and fibroblast activation signature genes (*Col1a1*, *Fn1*, etc.) in aortic fibroblasts from TKO mice (Figure 6C, S6B through E). Furthermore, calcium signaling related genes were also increased in TKO fibroblasts (Figure 6C). To further assess whether these fibrotic related changes were mediated by IL-9, primary aortic fibroblasts were isolated from C57BL/6 mice and supernatants from WT or KO CD4+T cells were

added to the fibroblasts grown in culture with and without anti-IL-9 antibodies (Figure 6D). Supernatants from KO CD4+T cells increased the expression of multiple fibrotic genes including *Col1a1, Col3a1, Col8a1, Acta2, Angptl1, Fmod*, and *Mmp9*, whereas anti-IL-9 antibodies reversed their expression (Figure 6E). Conversely, treatment of fibroblasts with recombinant IL-9 or Ang II increased the expression of *Col1a1*, *Col3a1*, *Col5a1, Acta2, and Mmp9*, and treatment with IL-9 plus Ang II together demonstrated additive effects (Figure 6F). Immunofluorescence also confirmed that IL-9, Ang II, or IL-9 plus Ang II additively increased the expression of Col1a1 and α-SMA (Figure 6G). Notably, there were no differences in expression of *IL9r* in any of the CD4+ T cell, fibroblast, or aortic tissue RNA-seq datasets (Figure S6F). Altogether, fibroblasts from TKO mice exhibit an activated fibroblast signature along with myofibroblast-related genes, which is recapitulated in C57BL/6 fibroblasts treated with IL-9 and Ang II.

Considering KLF10 is a putative regulator of transforming growth factor (TGF)-β signaling in specific disease states,[12, 13] we evaluated the expression of TGF-β isoforms in plasma. There were no differences in TGF-β1 or TGF-β2 in plasma between KO and Cre control mice treated with Ang II (Figure S7A). Despite a modest reduction in TGF-β3 in the plasma, there were no differences in expression levels for TGFβ1-3 between KO and Cre control CD4+ T cell supernatants (Figure S7A and S7B). In addition, examination for mediators of the TGF-β signaling pathway in our 3 RNA-seq datasets and 1 published T CD4+ cell dataset showed no impact of KLF10 on TGF-β signaling in vivo supported by pathway analyses from these 4 different RNA-seq datasets (Table S5). These findings suggest that the KLF10-mediated effects in CD4+ T cells on fibroblasts were likely independent of TGF-β signaling.

Single-cell RNA sequencing revealed fibroblast heterogeneity and activation signatures induced in TKO aortas.

To further understand the differences in phenotypic heterogeneity in fibroblasts during the progression of perivascular fibrosis between TKO and control mice in response to Ang II treatment, we performed single-cell RNA-sequencing (scRNA-seq) of the descending aorta (Figure 7A). A total of 53,346 cells from our four samples met quality control metrics (Figure S8A) and were integrated and analyzed. The Seurat package[31] was used for integration, clustering, and marker analysis (detailed in extended methods). We classified the cells in 10 major aortic cell types based on identified marker genes in each cluster (Figure S8B, S8C, S9A through S9D, and Table S6). The Uniform Manifold Approximation and Projection (UMAP) with the labeled clusters are shown in Figure 7B and Figure S9B. The percentage and the number of aortic cells from TKO and Cre aorta in each cell type are shown in Figure 7C, S9E, and Table S7. Considering the important biological role of fibroblasts in perivascular fibrosis, fibroblasts in the integrated dataset were identified by established markers such as platelet-derived growth factor receptor-α (Pdgfrα)[32, 33] (Figure S10A). Notably, we found that both the percentage and the number of fibroblasts increased in Ang II-treated TKO aortas compared to Cre controls (Figure 7C, **9E**, and Table S7). Differential expression analysis between TKO and Cre aortas in the fibroblast clusters revealed a total of 627 DEGs. Pathway enrichment analysis of these DEGs highlighted several pathways associated with fibrosis in the TKO aorta including extracellular matrix

(ECM), ECM organization, and collagen fibril and extracellular fibril organization (Figure 7D). Considering the important biological role of fibroblasts in the production of the enriched ECM[34], we assessed for relative changes in fibroblast activation signature genes, collagen family genes, and matrix metalloproteinases (MMPs) between TKO and Cre aorta controls, and found that many were upregulated in the Ang II treated TKO group (Figure S10B).

Further subsetting and cluster analysis[31] was performed in the fibroblast group and 9 fibroblast subclusters (FBS) were identified based on the unique enriched markers (Figure 7E, S10C, S10D, S11, Table S8). Specifically, FBS_1 and FBS_2 showed high expression of *Pdgfa,* a canonical fibroblast marker that was found in perivascular regions rarely overlapping with αSMA[35]; FBS_3 and FBS_4 were enriched in lymphocyte markers; FBS_5 was an EC-like fibroblast cluster that highly expressed *Cdh5* and *Kdr*[36, 37], suggesting potential endothelial-mesenchymal transition during fibrosis [38, 39]; FBS_6 highly expressed *Col4a5*, a collagen marker that was found to be related to a matrix fibroblast signature with endoplasmic reticulum stress activation[40, 41]; FBS_7 highly expressed *Mmps,* also considered as matrix fibroblasts highly expressing *Mmp3*[41, 42]; FBS_8 highly expressed *Col8a1, Col11a1, Angptl1,*and *Cthrc1*, and was considered as a group of collagen-related pathological fibroblasts that are activated[43-46]; and FBS_9 highly expressed *Lyz2* and *Ccl6*, considered as a group of inflammation-related activated fibroblasts[32] (Figure.S11). A differential abundance analysis for the conditions in each fibroblast subcluster showed a decrease in FBS_2 (log2FC = −1.18, adj. pval = 0.04), while there was an increase in the number of cells in FBS_8 (log2FC = 1.64, adj. pval = 0.01) from the aorta of Ang II-treated TKO mice compared to Cre control (Figure 7F, S12A, and Table S9). Interestingly, the increased FBS subclusters (FBS_8) in TKO mice were highly associated with pathological or disease enriched fibrosis-related genes (Figure 7G, Table S10). A combined gene score using a previously defined fibrosis-related gene list (Table S11) showed that FBS_8 had the highest score among all the FBS subclusters, suggesting the FBS_8 was a key fibrosis-driven subcluster (Figure 7H). In contrast, a combined gene score using a group of canonical fibroblast genes (Table S11) showed that FBS_2 had the highest score, suggesting that FBS_2 may be the canonical type of fibroblast (Figure S12B).

We next performed RNA velocity analysis, a method which calculates both spliced and unspliced mRNA counts to predict potential future directionality and speed of cell state transitions[47]. Higher proportions of unspliced to spliced mRNA highlights the active transcription state within a given cell cluster. Using this analysis, we obtained a trajectory of the different FBS subclusters states (Figure 7I). FBS_2 appeared to be the initial state of FBS in the stream plot (Figure 7I), which was consistent with our previous observation on the enriched markers of canonical FBS genes in FBS_2. Following the paths from FBS_2 in the stream plot, we observed FBS_8 as the most progressed state from FBS_2 (Figure 7I).

Together with the observation of a higher percentage of cells in FBS_8 in TKO samples and fibrosis-related gene markers for this subcluster, FBS_8 is likely the most important cluster contributing to the perivascular fibrosis in TKO mice. Furthermore, k-means cluster analyses confirmed FBS_8 is completely different with FBS_1-5 and FBS_9 (Figure 7J). Further pathway analysis found that FBS_8 is highly involved in extracellular matrix and

structure organization (Figure 7K). Since Col8a1 is one of the unique collagen-related genes in FBS_8, we assessed its expression by co-staining with PDGFRα in the aorta. The Immunofluorescence staining result showed that Col8a1+PDGFRα+ cells were located in the perivascular area and the expression of Col8a1 increased in Ang II treated-TKO group (Figure 7L). Interestingly, we also found that *Col8a1* increased in the aortic fibroblasts from TKO mice after overlapping transcripts between the fibroblast upregulated DEGs from the scRNA-seq dataset and the upregulated DEGs from the isolated fibroblast bulk RNA-seq dataset (Figure 7M). Taken together, scRNA-seq of aortas from Cre and TKO mice after Ang II treatment revealed fibroblast heterogeneity with activated signatures most prominent among FBS_8, and induction of pathways associated with robust ECM and perivascular fibrosis.

Neutralization of endogenous IL-9 reversed the Ang II-induced perivascular fibrosis and ameliorated injury of hypertension-related organs

Considering the crucial profibrotic role of IL-9 in Ang II-treated perivascular fibrosis and the elevated plasma levels observed in the TKO mice, we hypothesized that perivascular fibrosis might be rescued by administration of anti-IL-9 neutralizing monoclonal antibodies (mAbs) in Ang II-treated TKO mice (Figure 8A). TKO mice treated with anti-IL9 mAbs showed improved LV GLS (Figure 8B, Table S12), decreased PWV, and increased Circ Strain (Figure 8C) compared with the IgG treated Ang II group, while no difference was observed in PBS groups. In addition, the ratio of albumin/creatinine and the value of KIM-1 decreased after treatment with IL-9 mAb in Ang II group (Figure 8D). Furthermore, histopathology analyses revealed significantly decreased perivascular fibrosis in the aorta, heart, and kidney in the anti-IL-9 mAb treatment group, and reduced aortic adventitial collagen was also observed in the anti-IL-9 mAb treated Ang II group compared with the IgG treated Ang II group (Figure 8E, 8F and S13A through D). Moreover, the increased calcium deposition in the perivascular adventitia was reversed by treatment with anti-IL-9 mAb in Ang II-treated TKO mice (Figure S13E).

To further understand the transcriptomic changes associated with the rescue of perivascular fibrosis with anti-IL-9 mAbs, RNA-seq differential expression analysis was performed from the anti-IL9 mAbs vs IgG groups in non-stripped aortas from TKO mice after Ang II treatment (Figure S13F through I). By analyzing the overlap between upregulated genes in non-stripped aortas from Ang II-treated TKO vs Cre mice with the downregulated transcripts in the anti-IL-9 mAb-treated TKO aortas, we identified potential genes involved with reversal of perivascular fibrosis, including *Alox15* and *Hp* (Figure S12J). [48-50] We also compared the significant downregulated transcripts from the non-stripped aortic anti-IL-9 mAb treatment with the significant upregulated transcripts from aortic fibroblasts of Ang II treated TKO vs. Cre mice to identity transcripts uniquely changed in fibroblasts after anti-IL-9 mAb rescue (Figure 8G). Indeed, the profibrotic genes *Col8a1*, *Mmp2, Fmod,* and *Angptl1,* which were identified *as* significantly increased in TKO aortas and in isolated fibroblasts by both bulk RNA seq and scRNA seq (Figure 7M), were all decreased after treatment with anti-IL-9 mAbs (Figure 8G). In addition, these genes were observed as overlapping from the upregulated genes from scRNA-seq with the downregulated genes from anti-IL-9 mAb RNA-seq dataset (Figure 8H).

To further determine if anti-IL-9 mAbs could provide therapeutic benefit outside of the context of genetically modified mice, we treated C57BL/6 mice with Ang II and with or without anti-IL-9 mAbs. Treatment with anti-IL9 mAbs showed decreased PWV and increased Circ Strain compared with the IgG treated control group (Figure 8I). Furthermore, histopathology analyses revealed significantly decreased perivascular fibrosis and reduced aortic adventitial collagen in the aorta in the anti-IL-9 mAb treatment group compared with the IgG control group (Figure 8J-K).

Collectively, neutralization of endogenous IL-9 ameliorated the Ang II-induced dysfunction of hypertension-related organs and reversed perivascular fibrosis not only in TKO mice by suppressing the expression of profibrotic genes, but also in C57BL/6 mice.

Discussion

Accumulating studies reveal the critical role of T cells not only in hypertension and hypertensive cardiovascular injury, but also in interstitial and perivascular fibrosis.[6, 10, 11, 19, 51-54] A variety of cell surface receptors, enzymes, and transcription factors associated with T cells have been implicated in the development of hypertension and target organ damage.[11, 21, 23] However, the molecular events in T cells specifically driving perivascular fibrosis in response to Ang II remain poorly understood. In this study, we found that Ang II induced *Klf10* expression in CD4+ T cells *in vitro* and *in vivo*, suggesting the potential involvement of KLF10 in Ang II mediated end organ damage and possibly fibrosis. We found that Ang II treated TKO mice developed adverse cardiac remodeling reflected by impaired GLS[55], worse arterial stiffness (evaluated by PWV and Circ Strain)[56], and more kidney injury (evaluated by the levels of albuminuria and KIM-1 expression)[23]. Notably, the TKO mice exhibited marked perivascular fibrosis in hearts, aortas, and kidneys. However, we found that those functional and histopathological changes were independent of blood pressure. These findings build upon a broader role for KLF10 in CD4+ T cells in a range of chronic inflammatory disease states including atherosclerosis, insulin resistance, and fatty liver disease.[12, 13]

A prior report considered that hypertension, vascular remodeling, and subsequent end-organ damage not only can be induced by mechanical forces, but also can result from other forms of mediators independent of arterial pressure[57], which suggests that blood pressure alone is not sufficient to predict end organ damage in hypertension. Indeed, abnormalities in aortic stiffness and PWV are typically associated with hypertensive subjects well before phenotypic manifestations of cardiac hypertrophy or other end-organ damage. Furthermore, more accurate clinical diagnostics are needed to detect early end organ damage in hypertensive patients.[58] Surprisingly, we did not find any differences in cardiac hypertrophy or interstitial fibrosis between Ang II-induced TKO and Cre control mice. Considering cardiac hypertrophy results from sustained pressure overload or heart injury [59], the lack of difference in blood pressure is consistent with the findings of similar extent of cardiac hypertrophy between TKO and Cre mice. The lack of difference in blood pressure between TKO and Cre also allowed us to leverage novel molecular insights into perivascular fibrosis.

Consistent with a prior finding[11], Ang II treatment increased the expression of the profibrotic cytokine IL-9 in both groups. Surprisingly, IL-9 was the only cytokine detected much higher in the TKO mice after Ang II treatment compared with Cre mice, which suggested that IL-9 played a crucial role in this perivascular fibrosis phenotype. IL-9 was reported in the regulation of immune responses and involved in the pathogenesis of various inflammatory diseases [60], including a profibrotic role in lung inflammation and fibrosis[61], liver fibrosis[62], and kidney fibrosis[63]. In cardiovascular disease, IL-9 has been implicated in the pathogenesis of atherosclerosis (exerting pro-atherosclerotic effects) [64] and in heart failure (aggravating isoproterenol-induced heart failure) [65]. To confirm the profibrotic role for IL-9 in Ang II-induced perivascular fibrosis, we systemically administrated recombinant murine IL-9 in Ang II-treated Cre mice and found that it increased perivascular fibrosis and induced dysfunction in heart, kidney, and aortas, which effectively phenocopied that observed in Ang II-treated TKO mice. Importantly, both the end organ injury and perivascular fibrosis were rescued by administration of anti-IL-9 neutralizing monoclonal antibodies in Ang II-treated TKO mice. Future studies evaluating the kinetics of IL-9 in plasma, CD4+ T cells, or PBMCs of hypertensive human subjects with increasing severity of end organ injury will be informative. Taken together, blocking IL-9 may be an attractive novel therapeutic strategy for treatment of perivascular fibrosis or hypertensive-associated end organ damage.

The main cellular sources of IL-9 are T cell subsets, including Th2, Treg, and from recently identified Th9 cells.[60] Consistently, flow cytometry also found that the percentage of CD4+IL9+ and CD4+IL4+ T cells increased in the aortic tissue and spleen in Ang II-infused TKO mice compared with Cre mice, while there were no differences in CD4+IL17+, CD4+FoxP3+, or CD4+ IFN-γ+ T cells. Although the percentage of CD4+IL4+ cells increased in TKO mice, there were no differences of released IL-13, IL-5, or IL-4 in both male and female TKO mice compared with Cre controls. In addition, using flow cytometry we found there was no difference in the percentage of CD8+IL-9+ cells between Ang II treated Cre and TKO mice in both aorta and spleen. Furthermore, we found increased transcript and protein expression of IL-9 in both isolated CD4+T cells from Ang II-infused TKO mice *in vivo* and Ang II-treated primary TKO CD4+T cells *in vitro*, which suggested that KLF10 may directly regulate IL-9 expression in CD4+ T cells. Unlike many other transcription factors, KLF10 is primarily known to repress transcription of targeted genes. For example, KLF10 can negatively regulate cardiac MCP-1 expression by blinding to the MCP-1 promoter with HDAC1.[24] Moreover, KLF10 can reduce acetylated histone H4 on the C/EBPα promoter and inactivate C/EBPα transcription.[66] In our study, we found that KLF10 can bind to the IL-9 promoter and interact with HDAC1 to inhibit *Il9* transcription. These findings suggest that the Ang II-mediated increase in KLF10 expression in CD4+ T cells may serve a protective, counter-regulatory mechanism to limit perivascular fibrosis. However, this increase is likely not sufficient to inhibit IL-9 release completely and can still trigger perivascular fibrosis. As a pro-fibrotic cytokine, IL-9 could also be regulated by multiple factors. As a tonic repressor of IL-9, KLF10 once deleted in CD4+ T cells triggers more IL-9 production and subsequently perivascular fibrosis. Further exploration of the interaction between KLF10, IL-9, and the promoters of other relevant targets may provide insights for the role of KLF10 more broadly in health and disease.

Ang II treatment, as a pathological stress, increases intracellular calcium to stimulate fibroblasts to differentiate into myofibroblasts, which can further induce fibrosis by secreted ECM proteins, MMPs, and others. [67] In our study, we found that fibrosis related signaling, ECM related pathways, and calcium signaling were particularly upregulated in Ang II-treated TKO mice compared with Cre control mice by RNA-seq. Given that calcium homeostasis is important in pulmonary fibroblasts [68] and cardiac fibroblasts [29, 67], we isolated aortic fibroblasts and found myofibroblast markers, fibroblast activation signature genes, and calcium signaling genes to be highly expressed from Ang II-treated TKO fibroblasts by RNA-seq. In particular, we show for the first time that IL-9 can also stimulate increased calcium flux and fibrosis phenotypes in isolated primary fibroblasts under basal and Ang II treatment. Thus, the IL-9 mediated perivascular fibrosis may be dependent in part on hyperactivation of calcium signaling in fibroblasts.

Fibroblasts are important cells involved in the maintenance of tissue integrity and tissue repair in response to injury.[69] They can differentiate into different phenotypes including an ECM-producing contractile phenotype that further contributes to the secretion and accumulation of ECM and MMPs leading to the progression of fibrosis in a range of fibrotic diseases. An appreciation of fibroblast heterogeneity within disease-specific conditions developed only recently with the advent of newly developed approaches using single cell transcriptome analysis. By using scRNA-seq, TKO aortic fibroblasts subsets exhibited higher activation markers including *Col1a1*, *Col8a1*, and *Col1a2*. Furthermore, nine identified subpopulations of fibroblasts displayed different aspects of fibroblast activation in TKO aortas, which demonstrated their relevance to perivascular fibrosis. In addition, in the Ang II-treated TKO aortas, the percentage of fibroblasts increased and the number and the percentages of specific FBS clusters were more abundant especially FBS_8. FBS_8 shows high expression of collagen-related genes including: *Cthrc1*, a potential marker for activated fibroblasts in the heart and lungs[45, 70, 71]; *Tnc*, a marker involved in stimulating collagen-related gene expression, myofibroblast transformation,[72] and perivascular inflammation and fibrosis[73]; and *Ddah1*, a marker related to perivascular or adventitial fibrosis and vascular remodeling[74]. Using RNA velocity analyses, FBS_8 represented one of the most advanced fibroblast clusters, while FBS_2 appeared as an earlier state reflecting less activation. Indeed, our results showed that FBS_8 is highly involved in the extracellular matrix and structure organization pathway and highly enriched for fibrosis-related genes, whereas FBS_2 was enriched for most of the canonical fibroblast genes. Col8a1 was found to be a unique gene in FBS_8, and Col8a1+ PDGFRα+ cells were located in the perivascular area and the expression of Col8a1 increased in the Ang II treated-TKO group. Thus, we consider the FBS_8 subcluster as the key fibroblast subcluster contributing to the perivascular fibrosis in the Ang II treated-TKO group. In addition, the majority of the other increased genes in the TKO group are known to contribute to the development of fibrosis,[43, 75-79] including *Col1a1*, *Mmp2*, *Angptl1*, *Comp*, *Fmod,* and *Acta2*—all decreased after administration of anti-IL-9 mAbs. Collectively, this anti-IL-9 therapeutic strategy demonstrated reduced end-organ injury and perivascular fibrosis in part by downregulating these fibrosis-related gene signatures.

In summary, *KLF10* is upregulated in PBMCs of hypertensive patients and in peripheral CD3+ T cells and CD4+ T cells in Ang II-treated mice. Administration of Ang II in

TKO mice triggered perivascular fibrosis, multi-organ dysfunction in heart, kidney, and aorta, and release of IL-9 from CD4+ T cells. These functional and histopathological differences were independent of blood pressure between Ang II-treated TKO and Cre mice. Mechanistically, in response to Ang II treatment, KLF10 bound to the IL-9 promoter and interacted with HDAC1 to inhibit IL-9 transcription. Ectopic IL-9 activated calcium flux, induced fibroblast activation and differentiation, increased production of collagen and ECM, thereby promoting the progression of perivascular fibrosis and inducing target organ dysfunction. Importantly, IL-9 neutralizing antibodies potently rescued perivascular fibrosis, and target organ dysfunction in Ang II treated TKO and C57BL/6 mice. RNA-seq and scRNA-seq revealed the presence of fibroblast heterogeneity and marked myofibroblast activation in non-stripped aortas from Ang II-treated TKO mice. These results indicate that the KLF10-IL-9 signaling axis in CD4+ T cells tightly regulate the processes of Ang II-induced pathological perivascular fibrosis and end organ damage and provide novel therapeutic opportunities for the treatment of hypertensive-associated disease.

Supplementary Material

Refer to Web version on PubMed Central for supplementary material.

Acknowledgments

We thank Dr. Lay-Hong Ang and Aniket P. Gad for their help with immunofluorescence imaging (Harvard Digestive Disease Center, NIH P30DK034854), and Dr. Sudeshna Fisch (Department of Medicine, Brigham and Women's Hospital Harvard Medical School) for assistance with echocardiography.

Sources of Funding

This work was supported by the National Institutes of Health (HL115141, HL134849, HL148207, HL148355, HL153356 to M.W.F.), and the American Heart Association (18SFRN33900144 and 20SFRN35200163 to M.W.F.).

Non-standard Abbreviations and Acronyms

Ang II	angiotensin II
TKO	CD4-targeted KLF10 deficient (Klf10fl/flCD4Cre+)
Cre	CD4-Cre (Klf10+/+CD4Cre+)
KLF10	Kruppel like factor 10
IL	interleukin
TFs	transcription factors
LV	left ventricular
PBMCs	peripheral blood mononuclear cells
GLS	global longitudinal strain
PWV	pulse-wave velocity
Circ Strain	circumferential strain

KIM-1	kidney injury molecule-1
HDAC1	histone deacetylase 1
DEGs	differentially expressed genes
TGF	transforming growth factor
scRNA-seq	single-cell RNA-sequencing
UMAP	uniform manifold approximation and projection
PDGFRα	platelet-derived growth factor receptor-α
ECM	extracellular matrix
MMPs	matrix metalloproteinases
FBS	fibroblast subclusters
mAbs	antibodies

References

1. Mitchell GF. Arterial stiffness and hypertension: Chicken or egg? Hypertension. 2014;64:210–214 [PubMed: 24799614]
2. McMaster WG, Kirabo A, Madhur MS, Harrison DG. Inflammation, immunity, and hypertensive end-organ damage. Circ Res. 2015;116:1022–1033 [PubMed: 25767287]
3. Wu J, Saleh MA, Kirabo A, Itani HA, Montaniel KR, Xiao L, Chen W, Mernaugh RL, Cai H, Bernstein KE, Goronzy JJ, Weyand CM, Curci JA, Barbaro NR, Moreno H, Davies SS, Roberts LJ, Madhur MS, Harrison DG. Immune activation caused by vascular oxidation promotes fibrosis and hypertension. J Clin Invest. 2016;126:1607
4. Mills KT, Stefanescu A, He J. The global epidemiology of hypertension. Nat Rev Nephrol. 2020;16:223–237 [PubMed: 32024986]
5. Lewington S, Clarke R, Qizilbash N, Peto R, Collins R. Age-specific relevance of usual blood pressure to vascular mortality: A meta-analysis of individual data for one million adults in 61 prospective studies. Lancet. 2002;360:1903–1913 [PubMed: 12493255]
6. Wu J, Saleh MA, Kirabo A, Itani HA, Montaniel KR, Xiao L, Chen W, Mernaugh RL, Cai H, Bernstein KE, Goronzy JJ, Weyand CM, Curci JA, Barbaro NR, Moreno H, Davies SS, Roberts LJ, 2nd, Madhur MS, Harrison DG. Immune activation caused by vascular oxidation promotes fibrosis and hypertension. J Clin Invest. 2016;126:50–67 [PubMed: 26595812]
7. Mikolajczyk TP, Nosalski R, Szczepaniak P, Budzyn K, Osmenda G, Skiba D, Sagan A, Wu J, Vinh A, Marvar PJ, Guzik B, Podolec J, Drummond G, Lob HE, Harrison DG, Guzik TJ. Role of chemokine rantes in the regulation of perivascular inflammation, t-cell accumulation, and vascular dysfunction in hypertension. Faseb j. 2016;30:1987–1999 [PubMed: 26873938]
8. Wenzel P, Knorr M, Kossmann S, Stratmann J, Hausding M, Schuhmacher S, Karbach SH, Schwenk M, Yogev N, Schulz E, Oelze M, Grabbe S, Jonuleit H, Becker C, Daiber A, Waisman A, Münzel T. Lysozyme m-positive monocytes mediate angiotensin ii-induced arterial hypertension and vascular dysfunction. Circulation. 2011;124:1370–1381 [PubMed: 21875910]
9. Guzik TJ, Touyz RM. Oxidative stress, inflammation, and vascular aging in hypertension. Hypertension. 2017;70:660–667 [PubMed: 28784646]
10. Guzik TJ, Hoch NE, Brown KA, McCann LA, Rahman A, Dikalov S, Goronzy J, Weyand C, Harrison DG. Role of the t cell in the genesis of angiotensin ii induced hypertension and vascular dysfunction. J Exp Med. 2007;204:2449–2460 [PubMed: 17875676]

11. Nosalski R, Siedlinski M, Denby L, McGinnigle E, Nowak M, Cat AND, Medina-Ruiz L, Cantini M, Skiba D, Wilk G, Osmenda G, Rodor J, Salmeron-Sanchez M, Graham G, Maffia P, Graham D, Baker AH, Guzik TJ. T-cell-derived mirna-214 mediates perivascular fibrosis in hypertension. Circ Res. 2020;126:988–1003 [PubMed: 32065054]
12. Cao Z, Wara AK, Icli B, Sun X, Packard RR, Esen F, Stapleton CJ, Subramaniam M, Kretschmer K, Apostolou I, von Boehmer H, Hansson GK, Spelsberg TC, Libby P, Feinberg MW. Kruppel-like factor klf10 targets transforming growth factor-beta1 to regulate cd4(+)cd25(−) t cells and t regulatory cells. J Biol Chem. 2009;284:24914–24924 [PubMed: 19602726]
13. Wara AK, Wang S, Wu C, Fang F, Haemmig S, Weber BN, Aydogan CO, Tesmenitsky Y, Aliakbarian H, Hawse JR, Subramaniam M, Zhao L, Sage PT, Tavakkoli A, Garza A, Lynch L, Banks AS, Feinberg MW. Klf10 deficiency in cd4(+) t cells triggers obesity, insulin resistance, and fatty liver. Cell Rep. 2020;33:108550 [PubMed: 33378664]
14. Astle WJ, Elding H, Jiang T, Allen D, Ruklisa D, Mann AL, Mead D, Bouman H, Riveros-Mckay F, Kostadima MA, Lambourne JJ, Sivapalaratnam S, Downes K, Kundu K, Bomba L, Berentsen K, Bradley JR, Daugherty LC, Delaneau O, Freson K, Garner SF, Grassi L, Guerrero J, Haimel M, Janssen-Megens EM, Kaan A, Kamat M, Kim B, Mandoli A, Marchini J, Martens JHA, Meacham S, Megy K, O'Connell J, Petersen R, Sharifi N, Sheard SM, Staley JR, Tuna S, van der Ent M, Walter K, Wang SY, Wheeler E, Wilder SP, Iotchkova V, Moore C, Sambrook J, Stunnenberg HG, Di Angelantonio E, Kaptoge S, Kuijpers TW, Carrillo-de-Santa-Pau E, Juan D, Rico D, Valencia A, Chen L, Ge B, Vasquez L, Kwan T, Garrido-Martín D, Watt S, Yang Y, Guigo R, Beck S, Paul DS, Pastinen T, Bujold D, Bourque G, Frontini M, Danesh J, Roberts DJ, Ouwehand WH, Butterworth AS, Soranzo N. The allelic landscape of human blood cell trait variation and links to common complex disease. Cell. 2016;167:1415–1429.e1419 [PubMed: 27863252]
15. Sela S, Mazor R, Amsalam M, Yagil C, Yagil Y, Kristal B. Primed polymorphonuclear leukocytes, oxidative stress, and inflammation antecede hypertension in the sabra rat. Hypertension. 2004;44:764–769 [PubMed: 15452031]
16. Siedlinski M, Jozefczuk E, Xu X, Teumer A, Evangelou E, Schnabel RB, Welsh P, Maffia P, Erdmann J, Tomaszewski M, Caulfield MJ, Sattar N, Holmes MV, Guzik TJ. White blood cells and blood pressure: A mendelian randomization study. Circulation. 2020;141:1307–1317 [PubMed: 32148083]
17. Klose CS, Diefenbach A. Transcription factors controlling innate lymphoid cell fate decisions. Curr Top Microbiol Immunol. 2014;381:215–255 [PubMed: 25038936]
18. Cao Z, Sun X, Icli B, Wara AK, Feinberg MW. Role of kruppel-like factors in leukocyte development, function, and disease. Blood. 2010;116:4404–4414 [PubMed: 20616217]
19. Barhoumi T, Kasal DA, Li MW, Shbat L, Laurant P, Neves MF, Paradis P, Schiffrin EL. T regulatory lymphocytes prevent angiotensin ii-induced hypertension and vascular injury. Hypertension. 2011;57:469–476 [PubMed: 21263125]
20. Bendall JK, Cave AC, Heymes C, Gall N, Shah AM. Pivotal role of a gp91(phox)-containing nadph oxidase in angiotensin ii-induced cardiac hypertrophy in mice. Circulation. 2002;105:293–296 [PubMed: 11804982]
21. Emmerson A, Trevelin SC, Mongue-Din H, Becker PD, Ortiz C, Smyth LA, Peng Q, Elgueta R, Sawyer G, Ivetic A, Lechler RI, Lombardi G, Shah AM. Nox2 in regulatory t cells promotes angiotensin ii-induced cardiovascular remodeling. J Clin Invest. 2018;128:3088–3101 [PubMed: 29688896]
22. Saleh MA, McMaster WG, Wu J, Norlander AE, Funt SA, Thabet SR, Kirabo A, Xiao L, Chen W, Itani HA, Michell D, Huan T, Zhang Y, Takaki S, Titze J, Levy D, Harrison DG, Madhur MS. Lymphocyte adaptor protein lnk deficiency exacerbates hypertension and end-organ inflammation. J Clin Invest. 2015;125:1189–1202 [PubMed: 25664851]
23. Norlander AE, Saleh MA, Pandey AK, Itani HA, Wu J, Xiao L, Kang J, Dale BL, Goleva SB, Laroumanie F, Du L, Harrison DG, Madhur MS. A salt-sensing kinase in t lymphocytes, sgk1, drives hypertension and hypertensive end-organ damage. JCI Insight. 2017;2
24. Yang J, Zhang H, Wang X, Guo J, Wei L, Song Y, Luo Y, Zhao Y, Subramaniam M, Spelsberg TC, Wang L, Xu W, Li M. Kruppel-like factor 10 protects against acute viral myocarditis by negatively regulating cardiac mcp-1 expression. Cell Mol Immunol. 2021;18:2236–2248 [PubMed: 32895486]

25. Mishra VK, Subramaniam M, Kari V, Pitel KS, Baumgart SJ, Naylor RM, Nagarajan S, Wegwitz F, Ellenrieder V, Hawse JR, Johnsen SA. Krüppel-like transcription factor klf10 suppresses tgfβ-induced epithelial-to-mesenchymal transition via a negative feedback mechanism. Cancer Res. 2017;77:2387–2400 [PubMed: 28249899]
26. Yang J, Zhang H, Wang X, Guo J, Wei L, Song Y, Luo Y, Zhao Y, Subramaniam M, Spelsberg TC. Kruppel-like factor 10 protects against acute viral myocarditis by negatively regulating cardiac mcp-1 expression. Cellular & Molecular Immunology. 2021;18:2236–2248 [PubMed: 32895486]
27. Cao Z, Wara AK, Icli B, Sun X, Packard RR, Esen F, Stapleton CJ, Subramaniam M, Kretschmer K, Apostolou I. Kruppel-like factor klf10 targets transforming growth factor-β1 to regulate cd4+ cd25− t cells and t regulatory cells. Journal of Biological Chemistry. 2009;284:24914–24924 [PubMed: 19602726]
28. Lombardi AA, Gibb AA, Arif E, Kolmetzky DW, Tomar D, Luongo TS, Jadiya P, Murray EK, Lorkiewicz PK, Hajnóczky G, Murphy E, Arany ZP, Kelly DP, Margulies KB, Hill BG, Elrod JW. Mitochondrial calcium exchange links metabolism with the epigenome to control cellular differentiation. Nat Commun. 2019;10:4509 [PubMed: 31586055]
29. Gibb AA, Lazaropoulos MP, Elrod JW. Myofibroblasts and fibrosis: Mitochondrial and metabolic control of cellular differentiation. Circ Res. 2020;127:427–447 [PubMed: 32673537]
30. Lin BL, Matera D, Doerner JF, Zheng N, Del Camino D, Mishra S, Bian H, Zeveleva S, Zhen X, Blair NT, Chong JA, Hessler DP, Bedja D, Zhu G, Muller GK, Ranek MJ, Pantages L, McFarland M, Netherton MR, Berry A, Wong D, Rast G, Qian HS, Weldon SM, Kuo JJ, Sauer A, Sarko C, Moran MM, Kass DA, Pullen SS. In vivo selective inhibition of trpc6 by antagonist bi 749327 ameliorates fibrosis and dysfunction in cardiac and renal disease. Proc Natl Acad Sci U S A. 2019;116:10156–10161 [PubMed: 31028142]
31. Satija R, Farrell JA, Gennert D, Schier AF, Regev A. Spatial reconstruction of single-cell gene expression data. Nat Biotechnol. 2015;33:495–502 [PubMed: 25867923]
32. Guerrero-Juarez CF, Dedhia PH, Jin S, Ruiz-Vega R, Ma D, Liu Y, Yamaga K, Shestova O, Gay DL, Yang Z, Kessenbrock K, Nie Q, Pear WS, Cotsarelis G, Plikus MV. Single-cell analysis reveals fibroblast heterogeneity and myeloid-derived adipocyte progenitors in murine skin wounds. Nat Commun. 2019;10:650 [PubMed: 30737373]
33. Chen CL, Paul LN, Mermoud JC, Steussy CN, Stauffacher CV. Visualizing the enzyme mechanism of mevalonate diphosphate decarboxylase. Nat Commun. 2020;11:3969 [PubMed: 32769976]
34. Kendall RT, Feghali-Bostwick CA. Fibroblasts in fibrosis: Novel roles and mediators. Front Pharmacol. 2014;5:123 [PubMed: 24904424]
35. Crnkovic S, Marsh LM, El Agha E, Voswinckel R, Ghanim B, Klepetko W, Stacher-Priehse E, Olschewski H, Bloch W, Bellusci S, Olschewski A, Kwapiszewska G. Resident cell lineages are preserved in pulmonary vascular remodeling. J Pathol. 2018;244:485–498 [PubMed: 29359814]
36. Meng S, Lv J, Chanda PK, Owusu I, Chen K, Cooke JP. Reservoir of fibroblasts promotes recovery from limb ischemia. Circulation. 2020;142:1647–1662 [PubMed: 32820662]
37. Li G, Liang W, Ding P, Zhao Z. Sutural fibroblasts exhibit the function of vascular endothelial cells upon mechanical strain. Arch Biochem Biophys. 2021;712:109046 [PubMed: 34599905]
38. Piera-Velazquez S, Li Z, Jimenez SA. Role of endothelial-mesenchymal transition (endomt) in the pathogenesis of fibrotic disorders. The American journal of pathology. 2011;179:1074–1080 [PubMed: 21763673]
39. Zeisberg EM, Potenta SE, Sugimoto H, Zeisberg M, Kalluri R. Fibroblasts in kidney fibrosis emerge via endothelial-to-mesenchymal transition. Journal of the American Society of Nephrology. 2008;19:2282–2287 [PubMed: 18987304]
40. Wang C, Liang S, Xing S, Xu K, Xiao H, Deng H, Wang X, Chen L, Ding J, Wang F. Endoplasmic reticulum stress activation in alport syndrome varies between genotype and cell type. Front Genet. 2020;11:36 [PubMed: 32117450]
41. Xie T, Wang Y, Deng N, Huang G, Taghavifar F, Geng Y, Liu N, Kulur V, Yao C, Chen P, Liu Z, Stripp B, Tang J, Liang J, Noble PW, Jiang D. Single-cell deconvolution of fibroblast heterogeneity in mouse pulmonary fibrosis. Cell Rep. 2018;22:3625–3640 [PubMed: 29590628]
42. Youkilis JC, Bassnett S. Single-cell rna-sequencing analysis of the ciliary epithelium and contiguous tissues in the mouse eye. Exp Eye Res. 2021;213:108811 [PubMed: 34717927]

43. Skrbic B, Engebretsen KV, Strand ME, Lunde IG, Herum KM, Marstein HS, Sjaastad I, Lunde PK, Carlson CR, Christensen G, Bjørnstad JL, Tønnessen T. Lack of collagen viii reduces fibrosis and promotes early mortality and cardiac dilatation in pressure overload in mice. Cardiovasc Res. 2015;106:32–42 [PubMed: 25694587]
44. Jia D, Liu Z, Deng N, Tan TZ, Huang RY, Taylor-Harding B, Cheon DJ, Lawrenson K, Wiedemeyer WR, Walts AE, Karlan BY, Orsulic S. A col11a1-correlated pan-cancer gene signature of activated fibroblasts for the prioritization of therapeutic targets. Cancer Lett. 2016;382:203–214 [PubMed: 27609069]
45. Gladka MM, Molenaar B, de Ruiter H, van der Elst S, Tsui H, Versteeg D, Lacraz GPA, Huibers MMH, van Oudenaarden A, van Rooij E. Single-cell sequencing of the healthy and diseased heart reveals cytoskeleton-associated protein 4 as a new modulator of fibroblasts activation. Circulation. 2018;138:166–180 [PubMed: 29386203]
46. Kanisicak O, Khalil H, Ivey MJ, Karch J, Maliken BD, Correll RN, Brody MJ, SC JL, Aronow BJ, Tallquist MD, Molkentin JD. Genetic lineage tracing defines myofibroblast origin and function in the injured heart. Nat Commun. 2016;7:12260 [PubMed: 27447449]
47. La Manno G, Soldatov R, Zeisel A, Braun E, Hochgerner H, Petukhov V, Lidschreiber K, Kastriti ME, Lönnerberg P, Furlan A, Fan J, Borm LE, Liu Z, van Bruggen D, Guo J, He X, Barker R, Sundström E, Castelo-Branco G, Cramer P, Adameyko I, Linnarsson S, Kharchenko PV. Rna velocity of single cells. Nature. 2018;560:494–498 [PubMed: 30089906]
48. Krönke G, Reich N, Scholtysek C, Akhmetshina A, Uderhardt S, Zerr P, Palumbo K, Lang V, Dees C, Distler O, Schett G, Distler JH. The 12/15-lipoxygenase pathway counteracts fibroblast activation and experimental fibrosis. Ann Rheum Dis. 2012;71:1081–1087 [PubMed: 22267335]
49. Takahashi N, Kikuchi H, Usui A, Furusho T, Fujimaru T, Fujiki T, Yanagi T, Matsuura Y, Asano K, Yamamoto K, Ando F, Susa K, Mandai S, Mori T, Rai T, Uchida S, Arita M, Sohara E. Deletion of alox15 improves kidney dysfunction and inhibits fibrosis by increased pgd(2) in the kidney. Clin Exp Nephrol. 2021;25:445–455 [PubMed: 33595729]
50. Gunzer S, Kraus A, Buchroth I, Grüneberg M, Westermann C, Biskup S, Reunert J, Grünewald I, Marquardt T. Hypertransaminasemia and liver fibrosis associated with haptoglobin retention and anhaptoglobinemia in a paediatric patient. Liver Int. 2021;41:2427–2432 [PubMed: 34358398]
51. Pan XX, Wu F, Chen XH, Chen DR, Chen HJ, Kong LR, Ruan CC, Gao PJ. T-cell senescence accelerates angiotensin ii-induced target organ damage. Cardiovasc Res. 2021;117:271–283 [PubMed: 32049355]
52. Caillon A, Mian MOR, Fraulob-Aquino JC, Huo KG, Barhoumi T, Ouerd S, Sinnaeve PR, Paradis P, Schiffrin EL. Γδ t cells mediate angiotensin ii-induced hypertension and vascular injury. Circulation. 2017;135:2155–2162 [PubMed: 28330983]
53. Guzik TJ, Mikolajczyk T. In search of the t cell involved in hypertension and target organ damage. Hypertension. 2014;64:224–226 [PubMed: 24866136]
54. Li C, Sun X-N, Zeng M-R, Zheng X-J, Zhang Y-Y, Wan Q, Zhang W-C, Shi C, Du L-J, Ai T-J, Liu Y, Liu Y, Du L-L, Yi Y, Yu Y, Duan S-Z. Mineralocorticoid receptor deficiency in t cells attenuates pressure overload-induced cardiac hypertrophy and dysfunction through modulating t-cell activation. Hypertension. 2017;70:137–147 [PubMed: 28559389]
55. Fröjdh F, Fridman Y, Bering P, Sayeed A, Maanja M, Niklasson L, Olausson E, Pi H, Azeem A, Wong TC, Kellman P, Feingold B, Christopher A, Fukui M, Cavalcante JL, Miller CA, Butler J, Ugander M, Schelbert EB. Extracellular volume and global longitudinal strain both associate with outcomes but correlate minimally. JACC Cardiovasc Imaging. 2020;13:2343–2354 [PubMed: 32563637]
56. Safar ME. Arterial stiffness as a risk factor for clinical hypertension. Nat Rev Cardiol. 2018;15:97–105 [PubMed: 29022570]
57. Luft FC, Mervaala E, Müller DN, Gross V, Schmidt F, Park JK, Schmitz C, Lippoldt A, Breu V, Dechend R, Dragun D, Schneider W, Ganten D, Haller H. Hypertension-induced end-organ damage : A new transgenic approach to an old problem. Hypertension. 1999;33:212–218 [PubMed: 9931107]
58. Schmieder RE. End organ damage in hypertension. Dtsch Arztebl Int. 2010;107:866–873 [PubMed: 21191547]

59. van der Meer P, Gaggin HK, Dec GW. Acc/aha versus esc guidelines on heart failure: Jacc guideline comparison. J Am Coll Cardiol. 2019;73:2756–2768 [PubMed: 31146820]
60. Noelle RJ, Nowak EC. Cellular sources and immune functions of interleukin-9. Nat Rev Immunol. 2010;10:683–687 [PubMed: 20847745]
61. Sugimoto N, Suzukawa M, Nagase H, Koizumi Y, Ro S, Kobayashi K, Yoshihara H, Kojima Y, Kamiyama-Hara A, Hebisawa A, Ohta K. Il-9 blockade suppresses silica-induced lung inflammation and fibrosis in mice. Am J Respir Cell Mol Biol. 2019;60:232–243 [PubMed: 30240278]
62. de Lira Silva NS, Borges BC, da Silva AA, de Castilhos P, Teixeira TL, Teixeira SC, Dos Santos MA, Servato JPS, Justino AB, Caixeta DC, Tomiosso TC, Espindola FS, da Silva CV. The deleterious impact of interleukin 9 to hepatorenal physiology. Inflammation. 2019;42:1360–1369 [PubMed: 30887397]
63. Guo X, Cen Y, Wang J, Jiang H. Cxcl10-induced il-9 promotes liver fibrosis via raf/mek/erk signaling pathway. Biomed Pharmacother. 2018;105:282–289 [PubMed: 29860220]
64. Zhang W, Tang T, Nie D, Wen S, Jia C, Zhu Z, Xia N, Nie S, Zhou S, Jiao J, Dong W, Lv B, Xu T, Sun B, Lu Y, Li Y, Cheng L, Liao Y, Cheng X. Il-9 aggravates the development of atherosclerosis in apoe−/− mice. Cardiovasc Res. 2015;106:453–464 [PubMed: 25784693]
65. Yang Y, Xu C, Tang S, Xia Z. Interleukin-9 aggravates isoproterenol-induced heart failure by activating signal transducer and activator of transcription 3 signalling. Can J Cardiol. 2020;36:1770–1781 [PubMed: 32621886]
66. Liu Y, Peng WQ, Guo YY, Liu Y, Tang QQ, Guo L. Krüppel-like factor 10 (klf10) is transactivated by the transcription factor c/ebpβ and involved in early 3t3-l1 preadipocyte differentiation. J Biol Chem. 2018;293:14012–14021 [PubMed: 30026232]
67. Feng J, Armillei MK, Yu AS, Liang BT, Runnels LW, Yue L. Ca(2+) signaling in cardiac fibroblasts and fibrosis-associated heart diseases. J Cardiovasc Dev Dis. 2019;6
68. Janssen LJ, Mukherjee S, Ask K. Calcium homeostasis and ionic mechanisms in pulmonary fibroblasts. Am J Respir Cell Mol Biol. 2015;53:135–148 [PubMed: 25785898]
69. Wohlfahrt T, Rauber S, Uebe S, Luber M, Soare A, Ekici A, Weber S, Matei AE, Chen CW, Maier C, Karouzakis E, Kiener HP, Pachera E, Dees C, Beyer C, Daniel C, Gelse K, Kremer AE, Naschberger E, Stürzl M, Butter F, Sticherling M, Finotto S, Kreuter A, Kaplan MH, Jüngel A, Gay S, Nutt SL, Boykin DW, Poon GMK, Distler O, Schett G, Distler JHW, Ramming A. Pu.1 controls fibroblast polarization and tissue fibrosis. Nature. 2019;566:344–349 [PubMed: 30700907]
70. Ruiz-Villalba A, Romero JP, Hernández SC, Vilas-Zornoza A, Fortelny N, Castro-Labrador L, San Martin-Uriz P, Lorenzo-Vivas E, García-Olloqui P, Palacio M, Gavira JJ, Bastarrika G, Janssens S, Wu M, Iglesias E, Abizanda G, de Morentin XM, Lasaga M, Planell N, Bock C, Alignani D, Medal G, Prudovsky I, Jin YR, Ryzhov S, Yin H, Pelacho B, Gomez-Cabrero D, Lindner V, Lara-Astiaso D, Prósper F. Single-cell rna sequencing analysis reveals a crucial role for cthrc1 (collagen triple helix repeat containing 1) cardiac fibroblasts after myocardial infarction. Circulation. 2020;142:1831–1847 [PubMed: 32972203]
71. Tsukui T, Sun KH, Wetter JB, Wilson-Kanamori JR, Hazelwood LA, Henderson NC, Adams TS, Schupp JC, Poli SD, Rosas IO, Kaminski N, Matthay MA, Wolters PJ, Sheppard D. Collagen-producing lung cell atlas identifies multiple subsets with distinct localization and relevance to fibrosis. Nat Commun. 2020;11:1920 [PubMed: 32317643]
72. Bhattacharyya S, Wang W, Morales-Nebreda L, Feng G, Wu M, Zhou X, Lafyatis R, Lee J, Hinchcliff M, Feghali-Bostwick C, Lakota K, Budinger GR, Raparia K, Tamaki Z, Varga J. Tenascin-c drives persistence of organ fibrosis. Nat Commun. 2016;7:11703 [PubMed: 27256716]
73. Shimojo N, Hashizume R, Kanayama K, Hara M, Suzuki Y, Nishioka T, Hiroe M, Yoshida T, Imanaka-Yoshida K. Tenascin-c may accelerate cardiac fibrosis by activating macrophages via the integrin αvβ3/nuclear factor-κb/interleukin-6 axis. Hypertension. 2015;66:757–766 [PubMed: 26238448]
74. Hasegawa K, Wakino S, Tatematsu S, Yoshioka K, Homma K, Sugano N, Kimoto M, Hayashi K, Itoh H. Role of asymmetric dimethylarginine in vascular injury in transgenic mice overexpressing dimethylarginie dimethylaminohydrolase 2. Circ Res. 2007;101:e2–10 [PubMed: 17601800]

75. Blanc V, Riordan JD, Soleymanjahi S, Nadeau JH, Nalbantoglu I, Xie Y, Molitor EA, Madison BB, Brunt EM, Mills JC, Rubin DC, Ng IO, Ha Y, Roberts LR, Davidson NO. Apobec1 complementation factor overexpression promotes hepatic steatosis, fibrosis, and hepatocellular cancer. J Clin Invest. 2021;131
76. Carbone C, Piro G, Merz V, Simionato F, Santoro R, Zecchetto C, Tortora G, Melisi D. Angiopoietin-like proteins in angiogenesis, inflammation and cancer. Int J Mol Sci. 2018;19
77. Mormone E, Lu Y, Ge X, Fiel MI, Nieto N. Fibromodulin, an oxidative stress-sensitive proteoglycan, regulates the fibrogenic response to liver injury in mice. Gastroenterology. 2012;142:612–621.e615 [PubMed: 22138190]
78. Schulz JN, Nüchel J, Niehoff A, Bloch W, Schönborn K, Hayashi S, Kamper M, Brinckmann J, Plomann M, Paulsson M, Krieg T, Zaucke F, Eckes B. Comp-assisted collagen secretion--a novel intracellular function required for fibrosis. J Cell Sci. 2016;129:706–716 [PubMed: 26746240]
79. Peyser R, MacDonnell S, Gao Y, Cheng L, Kim Y, Kaplan T, Ruan Q, Wei Y, Ni M, Adler C, Zhang W, Devalaraja-Narashimha K, Grindley J, Halasz G, Morton L. Defining the activated fibroblast population in lung fibrosis using single-cell sequencing. Am J Respir Cell Mol Biol. 2019;61:74–85 [PubMed: 30848683]
80. Cambier L, Giani JF, Liu W, Ijichi T, Echavez AK, Valle J, Marbán E. Angiotensin ii-induced end-organ damage in mice is attenuated by human exosomes and by an exosomal y rna fragment. Hypertension. 2018;72:370–380 [PubMed: 29866742]
81. Végran F, Berger H, Boidot R, Mignot G, Bruchard M, Dosset M, Chalmin F, Rébé C, Dérangère V, Ryffel B, Kato M, Prévost-Blondel A, Ghiringhelli F, Apetoh L. The transcription factor irf1 dictates the il-21-dependent anticancer functions of th9 cells. Nat Immunol. 2014;15:758–766 [PubMed: 24973819]
82. Licona-Limón P, Henao-Mejia J, Temann AU, Gagliani N, Licona-Limón I, Ishigame H, Hao L, Herbert DR, Flavell RA. Th9 cells drive host immunity against gastrointestinal worm infection. Immunity. 2013;39:744–757 [PubMed: 24138883]
83. Mitchell C, Rahko PS, Blauwet LA, Canaday B, Finstuen JA, Foster MC, Horton K, Ogunyankin KO, Palma RA, Velazquez EJ. Guidelines for performing a comprehensive transthoracic echocardiographic examination in adults: Recommendations from the american society of echocardiography. J Am Soc Echocardiogr. 2019;32:1–64 [PubMed: 30282592]
84. Lee L, Cui JZ, Cua M, Esfandiarei M, Sheng X, Chui WA, Xu MH, Sarunic MV, Beg MF, van Breemen C, Sandor GG, Tibbits GF. Aortic and cardiac structure and function using high-resolution echocardiography and optical coherence tomography in a mouse model of marfan syndrome. PLoS ONE. 2016;11:e0164778 [PubMed: 27824871]
85. Mirabito KM, Hilliard LM, Wei Z, Tikellis C, Widdop RE, Vinh A, Denton KM. Role of inflammation and the angiotensin type 2 receptor in the regulation of arterial pressure during pregnancy in mice. Hypertension. 2014;64:626–631 [PubMed: 24935937]
86. del Campo L, Ferrer M. Wire myography to study vascular tone and vascular structure of isolated mouse arteries. Methods Mol Biol. 2015;1339:255–276 [PubMed: 26445795]
87. Ni H, Haemmig S, Deng Y, Chen J, Simion V, Yang D, Sukhova G, Shvartz E, Wara A, Cheng HS, Pérez-Cremades D, Assa C, Sausen G, Zhuang R, Dai Q, Feinberg MW. A smooth muscle cell-enriched long noncoding rna regulates cell plasticity and atherosclerosis by interacting with serum response factor. Arterioscler Thromb Vasc Biol. 2021;41:2399–2416 [PubMed: 34289702]
88. Chen J, Zhuang R, Cheng HS, Jamaiyar A, Assa C, McCoy M, Rawal S, Pérez-Cremades D, Feinberg MW. Isolation and culture of murine aortic cells and rna isolation of aortic intima and media: Rapid and optimized approaches for atherosclerosis research. Atherosclerosis. 2022;347:39–46 [PubMed: 35306416]
89. Tajima K, Ikeda K, Tanabe Y, Thomson EA, Yoneshiro T, Oguri Y, Ferro MD, Poon ASY, Kajimura S. Wireless optogenetics protects against obesity via stimulation of non-canonical fat thermogenesis. Nat Commun. 2020;11:1730 [PubMed: 32265443]
90. Shakya K, Ruskin HJ, Kerr G, Crane M, Becker J. Comparison of microarray preprocessing methods. Adv Exp Med Biol. 2010;680:139–147 [PubMed: 20865495]
91. Walter W, Sánchez-Cabo F, Ricote M. Goplot: An r package for visually combining expression data with functional analysis. Bioinformatics. 2015;31:2912–2914 [PubMed: 25964631]

92. Amezquita RA, Lun ATL, Becht E, Carey VJ, Carpp LN, Geistlinger L, Marini F, Rue-Albrecht K, Risso D, Soneson C, Waldron L, Pagès H, Smith ML, Huber W, Morgan M, Gottardo R, Hicks SC. Orchestrating single-cell analysis with bioconductor. Nat Methods. 2020;17:137–145 [PubMed: 31792435]

Novelty and significance

What is Known?

- Perivascular fibrosis, often associated with hypertension, accelerates vascular aging, mediates vascular stiffness, induces vascular remodeling and target organ dysfunction.
- Perivascular fibrosis has been linked to perivascular inflammation and T cell activation in hypertension, although the precise mechanisms are poorly understood.
- KLF10 expression in CD4+ T cells regulates atherosclerotic lesion formation, obesity, insulin resistance, and fatty liver in mouse models.

What New Information Does This Article Contribute?

- Deficiency of *Klf10* in CD4+ T cells enhanced perivascular fibrosis in hearts, aortas, and kidneys after Ang II infusion and promoted multi-organ dysfunction independent of blood pressure.
- KLF10 deficiency in CD4+ T cells increases IL-9 expression and release, activating calcium flux and inducing a fibroblast activation signature, thereby accelerating perivascular fibrosis and end-organ damage in Ang II treated mice.
- Neutralization of endogenous IL-9 potently rescued the Ang II-induced end-organ dysfunction and perivascular fibrosis in TKO and C57BL/6 mice.

Perivascular fibrosis, a hallmark for advanced vascular disease states often associated with elevated blood pressure (BP), vascular stiffness, adverse vascular remodeling, and end-organ dysfunction, is greatly dependent on perivascular inflammation and immune cells in hypertension. Deficiency of *Klf10* in CD4+ T cells triggered perivascular fibrosis, multi-organ dysfunction in heart, kidney, and aorta, and release of IL-9 from CD4+ T cells after Ang II infusion independent of blood pressure. In response to Ang II treatment, KLF10 bound to the IL-9 promoter and interacted with HDAC1 to inhibit IL-9 transcription. Ectopic IL-9 activated calcium flux, induced fibroblast activation and differentiation, increased production of collagen and ECM, thereby promoting the progression of perivascular fibrosis and inducing target organ dysfunction. Importantly, IL-9 neutralizing antibodies potently rescued perivascular fibrosis, and target organ dysfunction in Ang II treated TKO and C57BL/6 mice. RNA-seq and scRNA-seq revealed the presence of fibroblast heterogeneity and marked myofibroblast activation in non-stripped aortas from Ang II-treated TKO mice. These results indicate that the KLF10-IL-9 signaling axis in CD4+ T cells tightly regulate the processes of Ang II-induced pathological perivascular fibrosis and end-organ damage and provide novel therapeutic opportunities for the treatment of hypertensive-associated disease.

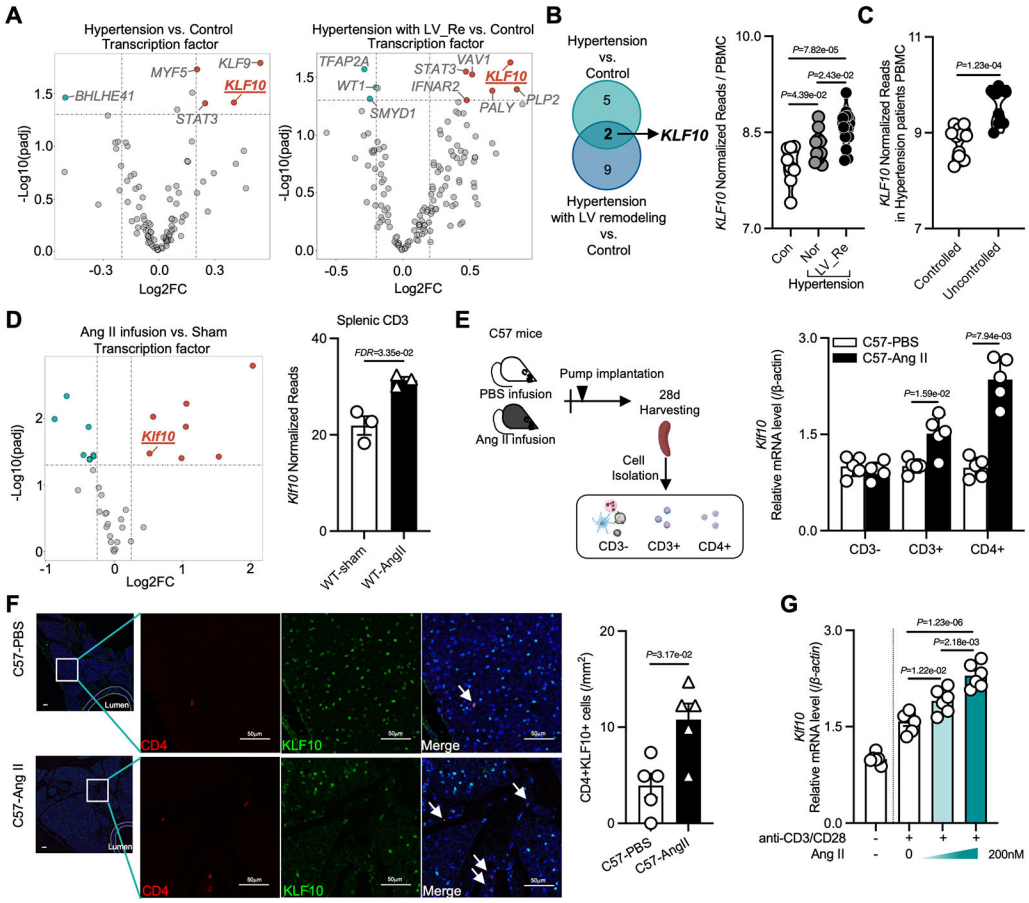

Figure 1. KLF10 expression is increased in T cells after Ang II treatment

A, Volcano plot highlighting regulated transcription factors in peripheral blood mononuclear cells (PBMCs) comparing hypertensive patients with normal left ventricular (LV) size and healthy controls (left), and hypertensive patients with LV remodeling and healthy controls (right). **B,** Venn diagram indicating the number of transcription factors regulated from two comparisons (left), and the normalized reads of *KLF10* in PBMCs from the healthy control group (n=8), hypertensive patients with or without LV remodeling (n=14 in each group). **C,** Normalized reads of *KLF10* in PBMCs from controlled (n=11) and uncontrolled hypertensives (n=9). **D,** Volcano plot highlighting regulated transcription factors in splenic CD3+ T cells (left), and the normalized reads of *Klf10* in splenic CD3+ T cells in sham and Ang II-treated mice. **E,** Schematic diagram of CD3−, CD3+ and CD4+ cell isolation from PBS or Ang II treated C57BL/6 mice, and the mRNA expression of *Klf10* in different cells (n=5). **F,** Representative Immunofluorescence staining, and the number of CD4+KLF10+ T cells in the adventitial regions in PBS or Ang II treated groups (n=5, scale bars =50μm). **G,** the expression of *Klf10* in Ang II treated CD4+ T cells. *P* values correspond to one-way ANOVA with Tukey's multiple comparisons tests (**B, G**), or unpaired two-tailed *t* tests (**C**). **D**, differentially expressed transcription factors were calculated by DEseq2 package. **E** and **F**, *P* values correspond to unpaired two-tailed Mann-Whitney *U*-tests. LV indicates left ventricle; Con, control; Nor, normal LV size; Re, remodeling; WT, wild type; Ang II, Angiotensin II.

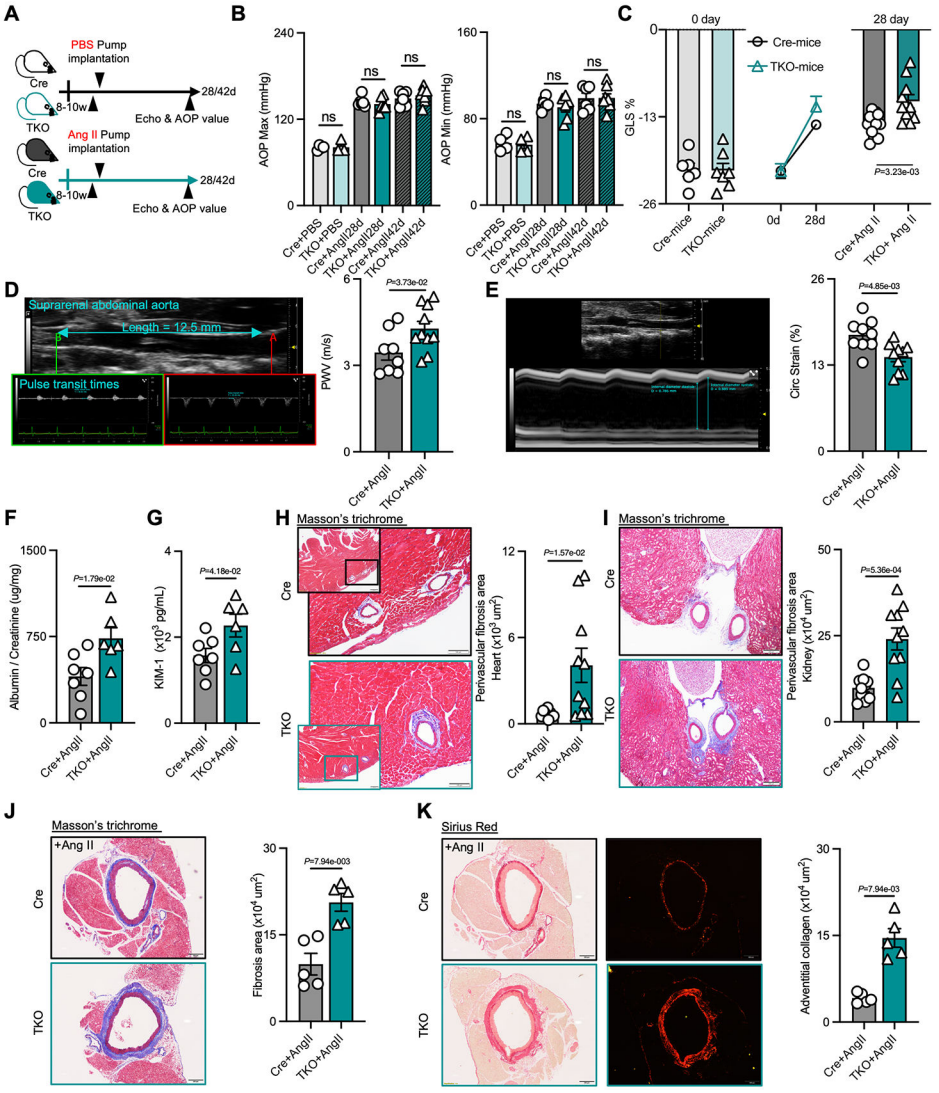

Figure 2. KLF10 deficiency in CD4+ T cells impairs the function of hypertension-related organs and triggers perivascular fibrosis independent of blood pressure.

A, Schematic diagram of experimental set-up of mice groups treated with PBS or Ang II infusion. **B**, Aortic blood pressure in Cre and TKO mice with PBS (n=4) or Ang II (n=6) treatment for 28 days or 42 days. **C**, Global longitudinal strain (GLS) in Cre and TKO mice before and after Ang II treatment (n=6 in Cre mice, n=7 in TKO mice, and n=10 in Ang II groups). **D-E**, Representative ultrasound imaging of the suprarenal abdominal aorta, and measurements of pulse wave velocity (PWV, **D**) and circumferential strain in Cre (n=8) and TKO mice (n=10) after 28 days of Ang II treatment. **F-G**, The ratio of albumin and creatinine (**F**), and the level of kidney injury molecule (KIM)-1 (**G**) in urine from Cre (n=7) and TKO mice (n=6) after Ang II treatment. **H-I**, Representative images of Masson trichrome staining, and quantification of perivascular fibrosis in the heart (**H**, scale bars =100μm) and kidney (**I**, scale bars= 200μm) (n=10). **J-K**, Representative images of Masson trichrome staining, and Sirius red staining and quantification of perivascular fibrosis and adventitial collagen in the aorta (n=5, scale bars= 200μm). **B-I**, *P* values

correspond to unpaired two-tailed *t* tests. **J** and **K**, *P* values correspond to unpaired two-tailed Mann-Whitney *U*-tests. Ang II indicates angiotensin II; Echo, echocardiogram; AOP, aortic pressure; ns, not significant; GLS, global longitudinal strain; PWV, pulse wave velocity; Circ Strain, circumferential strain; KIM-1, kidney injury molecule-1.

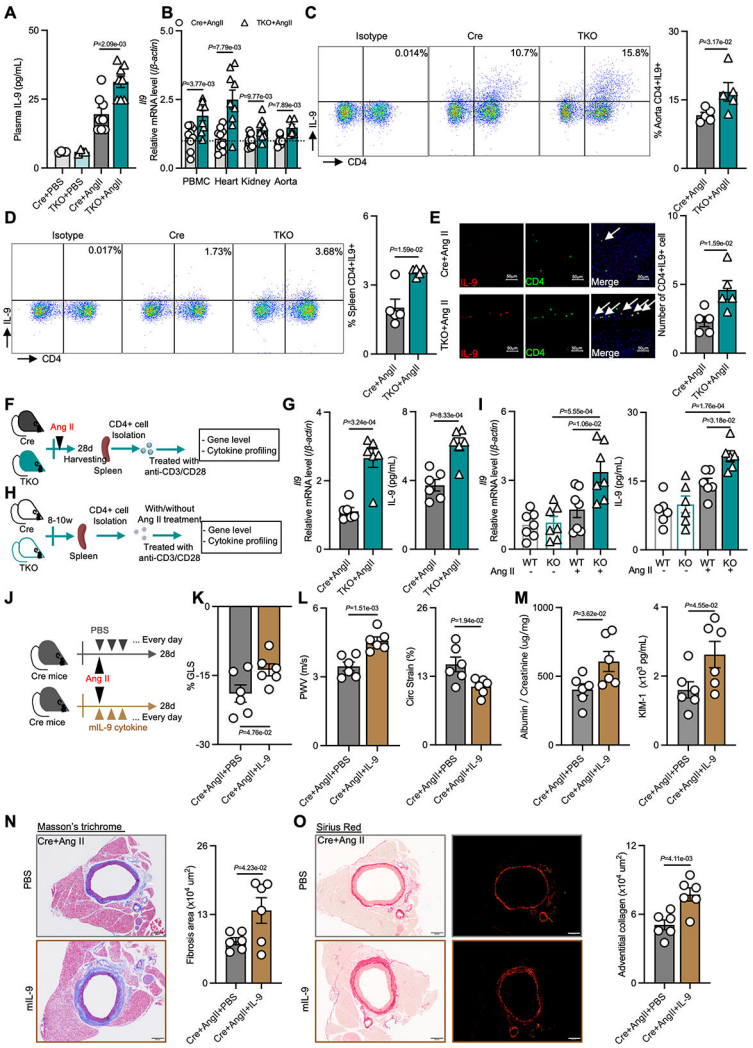

Figure 3. KLF10 deficient CD4+ T cells release IL-9 that mediates perivascular fibrosis

A, IL-9 levels were measured in plasma in PBS or Ang II treated Cre and TKO mice (n=4 in PBS groups, and n=8 in Ang II-treated groups). **B**, mRNA expression level of *Il9* in the PBMCs, heart, kidney, and aorta in Ang II-treated Cre and TKO mice (n=6 in aortic groups, and n=8 in others). **C-D**, Representative flow cytometry plots and the percentage of CD4+IL9+ T cells gated in CD3+ T cells in the aorta (**C**, n=5) and spleen (**D**, n=5). **E**, Representative immunofluorescence staining, and the number of CD4+IL9+ T cells in the aorta in Ang II treated Cre and TKO mice (n=5, scale bars= 50μm). **F-G**, Schematic diagram of the experimental setup for CD4+T cell isolation from Ang II-treated Cre or TKO mice (**F**), and quantification of *Il9 mRNA* in isolated CD4+ T cells, and IL-9 protein released into the supernatants of CD4+ T cells (**G**, n=6). **H-I**, Schematic diagram of the experimental setup of CD4+ T cell isolation from Cre control mice for *in vitro* treatment (**H**), quantification of *Il9 mRNA* in the treated CD4+ T cells, and IL-9 protein released into the supernatants of treated CD4+ T cells (**I**). **J**, Schematic diagram of the experimental setup for recombinant mIL-9 treatment in Cre mice. **K**, GLS in mIL-9 or PBS treated Cre mice after Ang II infusion (n=6). **L**, the value of PWV and circumferential strain in mIL-9

or PBS treated Cre mice after 28 days Ang II treatment (n=6). **M**, the ratio of albumin and creatinine, and the level of KIM-1 in urine in mIL-9 or IgG treated Cre mice after 28 days Ang II treatment (n=6). **N-O**, Representative images of Masson trichrome staining and Sirius red staining, and the area of perivascular fibrosis and adventitial collagen in the aorta (n=6, scale bars= 200μm). *P* values correspond to two-way ANOVA with Tukey's multiple comparisons tests (**A**, and **I**), or unpaired two-tailed *t* tests (**B**, **G**, and **K-O**). **C-E**, *P* values correspond to unpaired two-tailed Mann-Whitney *U*-tests. PBMC indicates peripheral blood mononuclear cells; Ang II, angiotensin II; GLS, global longitudinal strain; PWV, pulse wave velocity; Circ Strain, circumferential strain; KIM-1, kidney injury molecule-1.

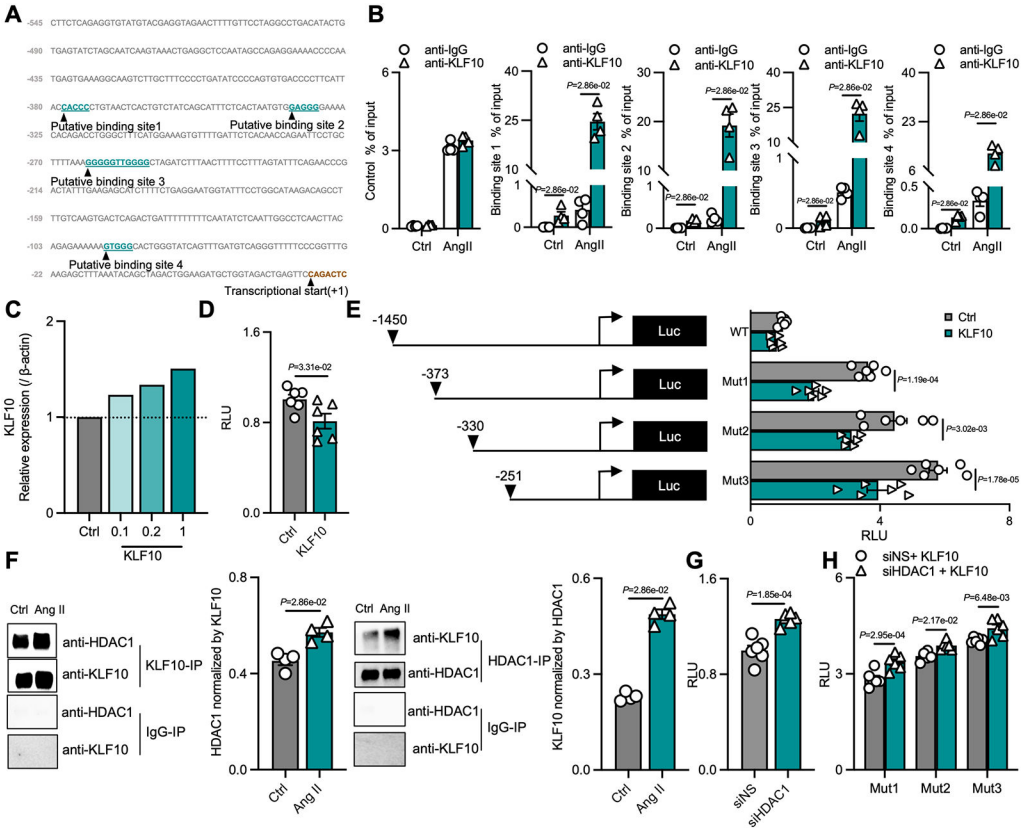

Figure 4. KLF10 binds to the IL-9 promoter and interacts with HDAC to inhibit IL-9 activation

A, Putative KLF10 transcription factor-binding sites in the mouse IL-9 promoter region. The putative binding sequences are highlighted. The transcription initiation site is defined as +1. **B**, Primary CD4+ T cells were isolated from Cre control mice and subjected to the chromatin immunoprecipitation (ChIP) assay with antibodies against IgG or KLF10. The immunoprecipitated DNA was subjected to semiquantitative PCR and q-PCR. **C**, The protein level of KLF10 after transfection. **D-E**, HEK293T cells were transfected with a full-length mouse IL-9 promoter luciferase reporter or 5' truncations of the IL-9 promoter, together with expression plasmids encoding full-length mouse KLF10 or empty vector (mock control). **F**, Primary CD4+ T cells were treated with Ang II for 12h, then cells were harvested, lysed, and subjected to immunoprecipitation by the indicated antibodies. Immunoprecipitation (IP) were subjected to Western blotting with the indicated antibodies, and the quantification of IP. **G-H**, HEK293T were co-transfected with mouse KLF10 expression vector and the indicated mouse IL-9 promoter luciferase reporters (WT, Mut1, Mut2, or Mut3), and siRNA (non-specific or HDAC1), and the relative luminescence units (RLU) after transfection. **B**, and **F**, *P* values correspond to unpaired two-tailed Mann-Whitney *U*-tests. For normal distributed data, *P* values correspond to unpaired two-tailed *t* tests (**D**, and **G**), or two-way ANOVA with Tukey's multiple comparisons tests (**E**, and **H**). Ctrl indicates control; Ang II, angiotensin II; Luc, luciferase reporters; RLU, relative luminescence units.

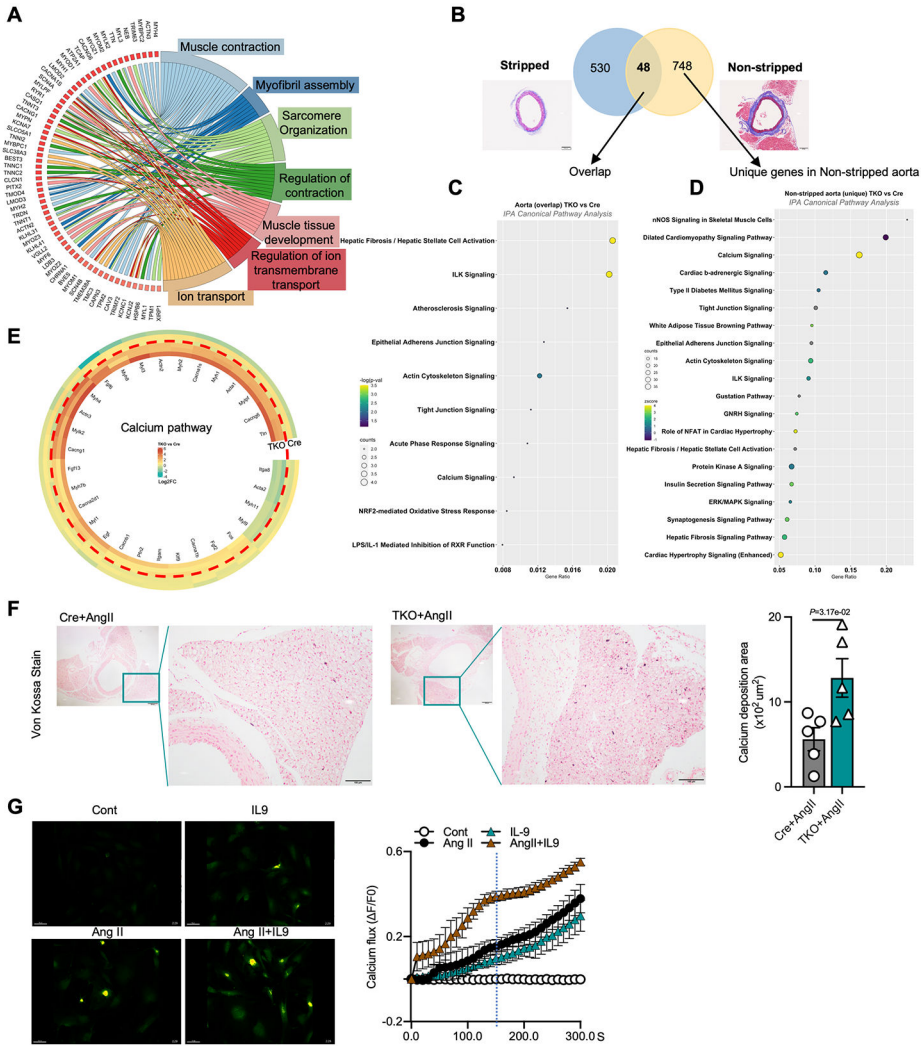

Figure 5. Transcriptomic changes involved in Ang II-induced perivascular fibrosis

A, GOChord plot showing the significantly regulated genes (log2 fold change >1.5; FDR <0.05) involved in the top 7 enriched pathways in non-stripped aorta. **B**, Differentially expressed genes in stripped and non-stripped aortas in Ang II treated Cre and TKO mice (FDR, <0.05). **C**, IPA Canonical pathway analysis after overlapping differentially expressed genes in stripped and non-stripped aortas. **D**, IPA Canonical pathway analysis by using unique differentially expressed genes in non-stripped aorta. **E**, Differentially expressed calcium pathway related genes. **F**, Representative images of Von Kossa staining, and the area of calcium deposition in the aorta (n=5, scale bars= 100μm). **G**, Real-time changes in intracellular calcium flux following IL-9, Ang II or Ang II and IL-9 treatment (Scale bars= 50 μm). **F**, *P* values correspond to unpaired two-tailed Mann-Whitney *U*-tests. Ang II indicates angiotensin II, Cont, Control.

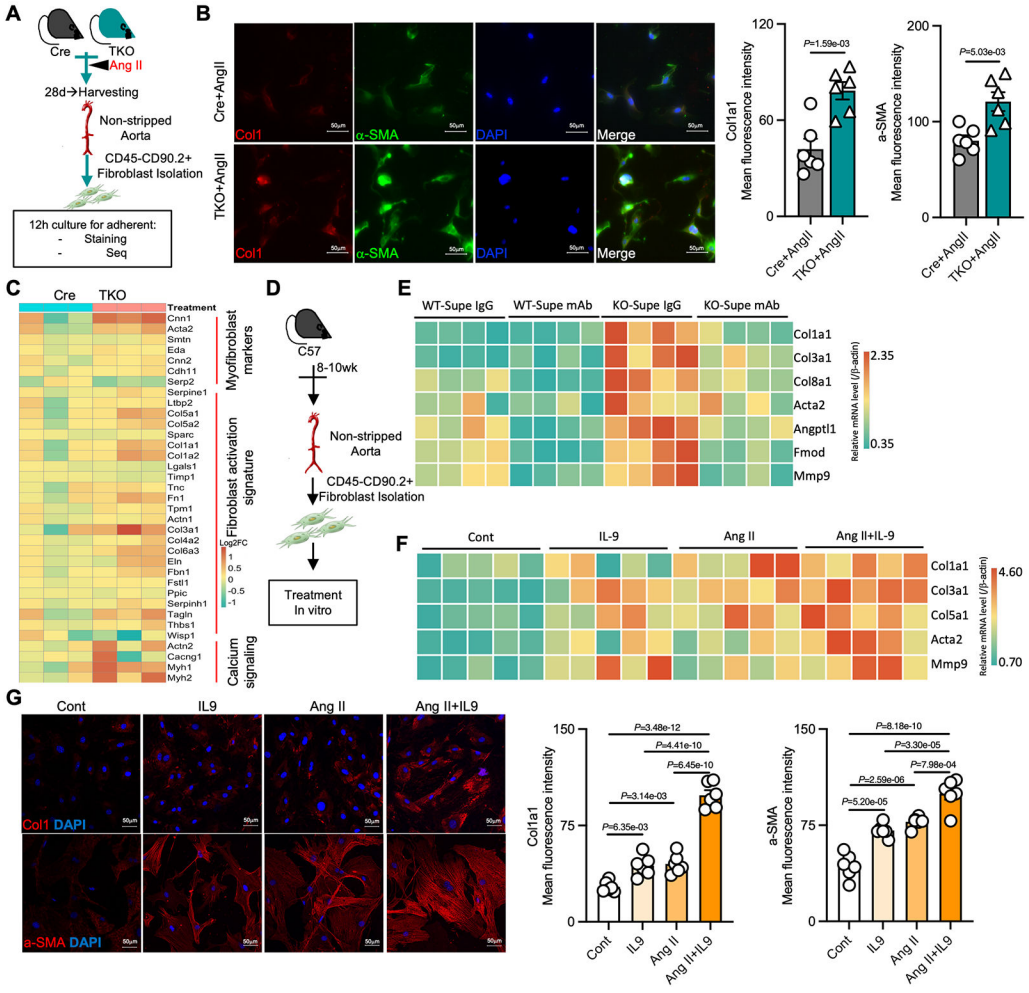

Figure 6. TKO fibroblasts display an activation signature and IL-9 and Ang II treatment recapitulate the phenotype in control fibroblasts

A, Schematic diagram of fibroblast isolation from Ang II-treated Cre or TKO mice. **B**, Representative immunofluorescence images, and the mean fluorescence intensity of Col1a1 and α-SMA in the isolated fibroblasts from Ang II-treated Cre or TKO mice (n=6, scale bars= 50 μm). **C**, Heatmap of dysregulated genes related to myofibroblast markers, fibroblast activation signature, and calcium signaling in isolated fibroblasts. **D**, Schematic diagram of primary aortic fibroblast isolation from C57BL/6 mice for further *in vitro* experiment. **E**, Gene expression of fibrotic markers in primary aortic fibroblasts grown in supernatants from KO or Cre CD4+T cells treated with Ang II in the presence of IgG or anti-IL-9 mAbs. **F**, Gene expression of fibrotic markers in primary aortic fibroblasts after treatment with IL-9, Ang II, or Ang II and IL-9 treatment. **G**, Representative immunofluorescence images, and the mean fluorescence intensity of Col1a1 and α-SMA in primary aortic fibroblasts after IL-9, Ang II, or Ang II and IL-9 treatment (n=6, scale bars= 50μm). *P* values correspond to an unpaired two-tailed *t* test (**B**), one-way ANOVA with Tukey's multiple comparisons tests (**G**). Ang II indicates angiotensin II.

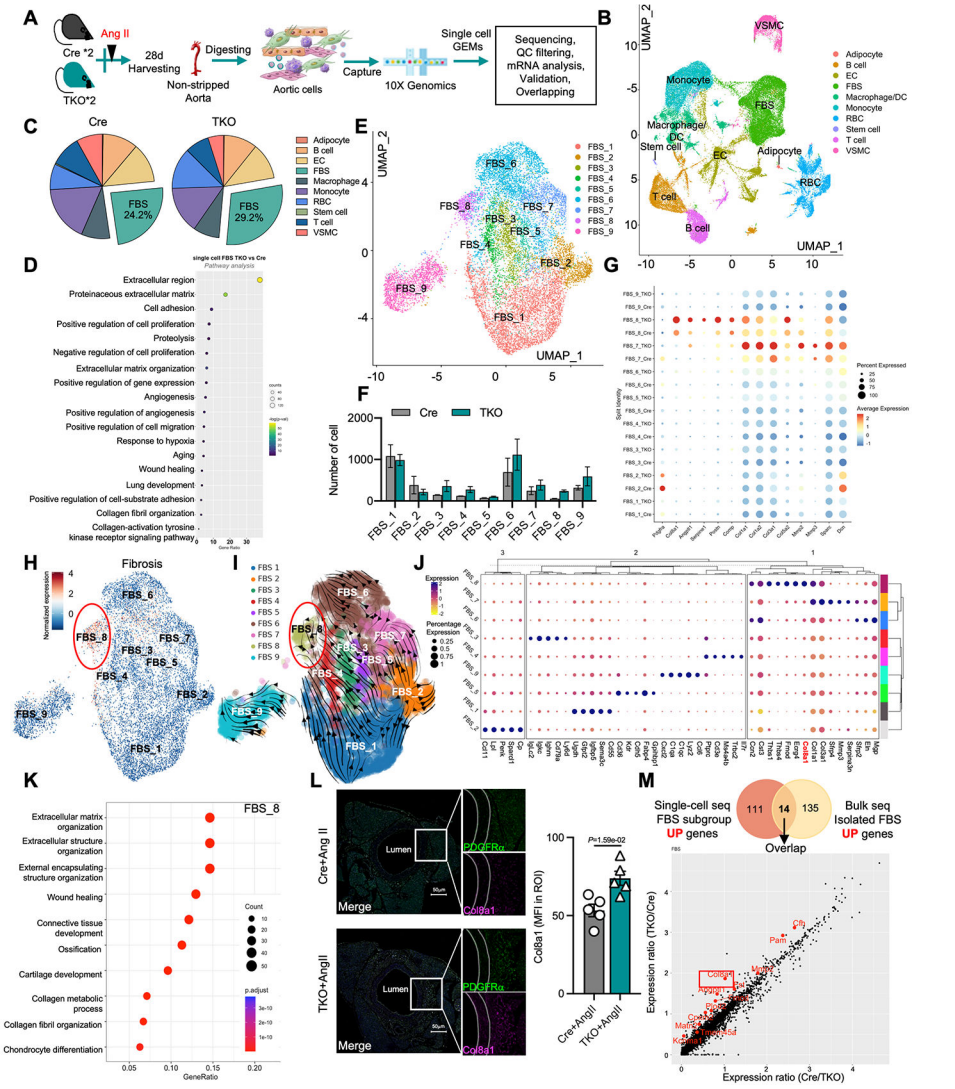

Figure 7. Single-cell RNA sequencing revealed fibroblast heterogeneity and activation signatures induced in TKO aortas.

A, Schematic diagram of aortic cells isolated from Ang II-treated Cre or TKO mice for single-cell RNA sequencing. **B**, Uniform Manifold Approximation and Projection (UMAP) of different aortic cell types. **C**, the percentage of different aortic cell types. **D**, IPA pathway analysis using total differentially expressed genes in fibroblasts. **E**, UMAP of 9 main fibroblast cell clusters. **F**, the number of different fibroblast clusters in Ang II treated Cre and TKO mice. **G**, dot plot of fibroblast activation signature-related genes. **H**, the UMAP of fibrosis genes by using add module score analysis. **I**, Velocity vector field displayed over the FBS UMAP. **J**, K-means cluster analysis for each fibroblast subclusters. **K**, Pathway analysis using the specific genes enriched in FBS_8. **L**, Representative immunofluorescence images of PDGFRα and Col8a1 in aorta (n=5, scale bars= 50μm). **M**, Overlapping upregulated genes from the indicated single-cell RNA seq dataset and isolated fibroblast bulk-RNA seq datasets (top); the overlapping increased genes from single-cell RNA seq (bottom). **L**, *P* values correspond to an unpaired two-tailed Mann-Whitney *U*-test. DC

indicates dendritic cells; FBS, fibroblasts; EC, endothelial cells; RBC, red blood cells; VSMC, vascular smooth muscle cells; Ang II, angiotensin II.

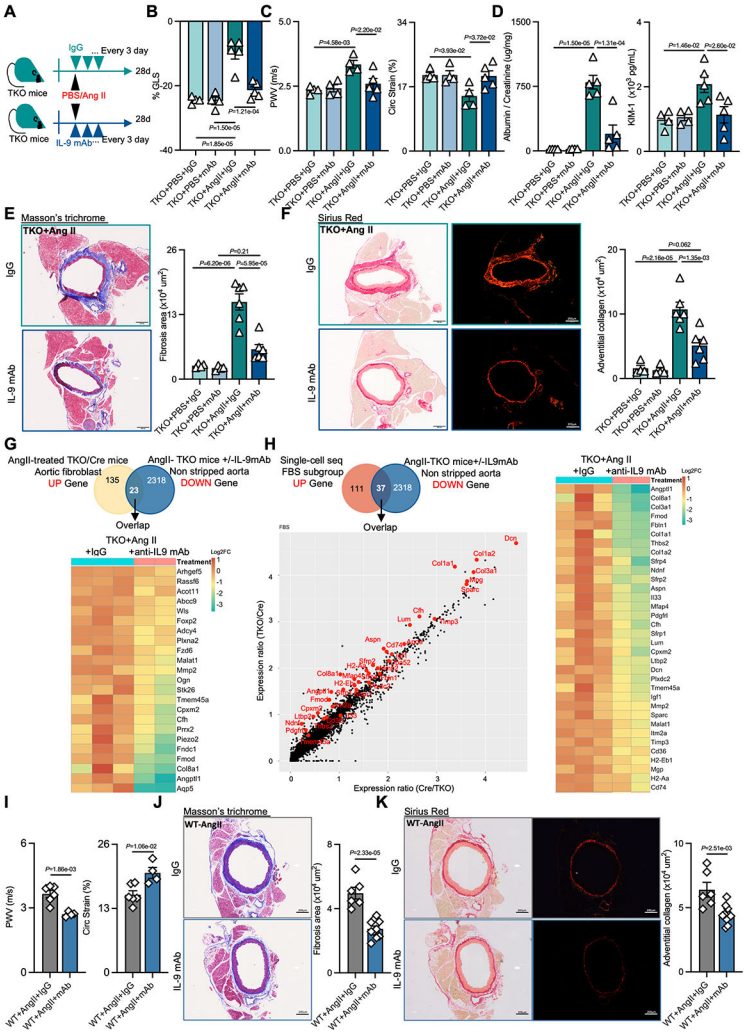

Figure 8. Neutralization of endogenous IL-9 reversed the Ang II-induced perivascular fibrosis and ameliorated injury of hypertension-related organs

A, Schematic diagram of the experimental setup for treatment with anti-IL-9 antibodies (mAb) in PBS or Ang II treated-TKO mice. **B-C**, Quantification of GLS (**B**), PWV and Circ Strain (**C**) in anti-IL-9 antibodies (mAb) or IgG treated TKO mice after 28 days PBS (n=4) or Ang II (n=5) infusion. **D**, The ratio of albumin and creatinine, and the level of KIM-1 in urine (n=4 in PBS groups, and n=5 in Ang II groups). **E-F**, Representative images of Masson trichrome staining and Sirius red staining, and quantification of perivascular fibrosis and adventitial collagen in the aorta (n=4 in PBS groups, n=6 in Ang II groups, scale bars= 200μm). **G**, Venn diagram of overlapping dysregulated genes from the upregulated genes from the isolated fibroblast bulk-RNA seq dataset and the downregulated genes in the anti-IL-9 mAb or IgG treated TKO mice bulk-RNA seq datasets (top), and the heatmap of downregulated genes in IL-9 mAb and IgG treated TKO mice non-stripped aortas after overlapping (bottom). **H**, Venn diagram of overlapping dysregulated genes from upregulated genes in the single cell-RNA seq dataset and the downregulated genes in the anti-IL-9 mAb or IgG treated TKO mice bulk-RNA seq datasets (top), the increased overlapping genes from single-cell seq (bottom), and the heatmap of downregulated overlapping genes in anti-IL-9

mAb and IgG treated of non-stripped aortas from TKO mice (right). **I**, quantification of PWV and Circ Strain in anti-IL-9 mAb (n=4) or IgG (n=5) treated WT mice after 28 days of Ang II treatment. **J-K**, Representative images of Masson trichrome staining and Sirius red staining, and quantification of perivascular fibrosis and adventitial collagen in the aorta in anti-IL-9 mAb (n=10) or IgG (n=6) treated WT mice after 28 days of Ang II treatment (scale bars= 200μm)., *P* values correspond to two-way ANOVA with Tukey's multiple comparisons tests (**B-F**), or unpaired two-tailed *t* tests (**I-K**). Ang II indicates angiotensin II; PWV, pulse wave velocity; Circ Strain, circumferential strain; KIM-1, kidney injury molecule-1.

Major Resources Table

In order to allow validation and replication of experiments, all essential research materials listed in the Methods should be included in the Major Resources Table below. Authors are encouraged to use public repositories for protocols, data, code, and other materials and provide persistent identifiers and/or links to repositories when available. Authors may add or delete rows as needed.

Animals (in vivo studies)

Species	Vendor or Source	Background Strain	Sex	Persistent ID / URL
Mouse	Charles River	C57BL/6	M	https://www.criver.com/products-services/find-model/c57bl6-mouse?region=3611

Genetically Modified Animals

Strain	Vendor or Source	Background Strain	Other Information	Persistent ID / URL
CD4-Cre *Klf10-flox*	Our laboratory (Laboratory of Mark W.Feinberg)	C57BL/6	———	Original Publication: [13]

Antibodies

Target antigen	Vendor or Source	Catalog #	Working concentration	Persistent ID / URL
Anti-mouse IL-9	Bio X Cell	BE0181	200ug per mouse	https://bxcell.com/product/m-il-9
Mouse IgG2a isotype control	Bix X Cell	BE0085		https://bxcell.com/product/invivomab-mouse-igg2a-isotype-control-unknown-specificity
Anti-KLF10	Invitrogen	PA5-19845	1 μg/mL	https://www.thermofisher.cn/cn/en/antibody/product/KLF10-Antibody-Polyclonal/PA5-19845
Anti-IL-9	Abcam	Ab227037	1:500	https://www.abcam.com/il-9-antibody-epr23484-151-ab227037.html
Anti- KLF10	Abcam	Ab73537	1 μg/ml	https://www.abcam.com/klf10-antibody-ab73537.html
Anti-KLF10	Santa Cruz Biotechnology	sc-130408	1:200	https://www.scbt.com/zh/p/tieg1-antibody-95-d?requestFrom=search
Anti-HDAC1	GeneTex	Gtx100513	1:100	https://www.genetex.cn/Product/Detail/HDAC1-antibody/GTX100513
Anti-CD4	Abcam	Ab183685	1:200	https://www.abcam.com/cd4-antibody-epr19514-ab183685.html
Anti-Col8a1	Abcam	Ab236653	1:200	https://www.abcam.com/col8a1-antibody-ab236653.html
Anti-PDGFRa	Thermo Scientific	MA541209	1:200	https://www.thermofisher.cn/cn/en/antibody/product/PDGFRA-Antibody-clone-JF104-6-Recombinant-Monoclonal/MA5-41209
Anti-Col1a1	Novus Biologicals	NBP1-30054	1:250	https://www.novusbio.com/products/collagen-i-alpha-1-antibody_nbp1-30054
Anti-aSMA	Sigma-Aldrich	A5228	1:500	https://www.sigmaaldrich.cn/CN/en/product/sigma/a5228
Cy3 conjugated donkey anti-rat secondary antibody	Jackson ImmunoResearch Lab	712-165153	1:300	https://www.jacksonimmuno.com/catalog/products/712-165-153
Alexa 647 conjugated donkey anti-rabbit secondary antibody	Jackson ImmunoResearch Lab	711-605152	1:300	https://www.jacksonimmuno.com/catalog/products/711-605-152

Antibodies

Target antigen	Vendor or Source	Catalog #	Working concentration	Persistent ID / URL
Alexa 488 conjugated donkey anti-rabbit secondary antibody	Jackson ImmunoResearch Lab	711-545152	1:300	https://www.jacksonimmuno.com/catalog/products/711-545-152
4′,6-diamidino-2-phenylindole(DAPI)	BioLegend	422801	300 nM	https://www.biolegend.com/en-us/products/dapi-4-6-diamidino-2-phenylindole-dilactate-8108?GroupID=BLG2181
PE Rat anti-Mouse CD90.2 antibody	BD Biosciences	553006	1:100	https://www.bdbiosciences.com/en-us/products/reagents/flow-cytometry-reagents/research-reagents/single-color-antibodies-ruo/pe-rat-anti-mouse-cd90-2.553006
BUV563 Rat anti-Mouse CD45	BD Biosciences	612924	1:100	https://www.bdbiosciences.com/en-us/products/reagents/flow-cytometry-reagents/research-reagents/single-color-antibodies-ruo/buv563-rat-anti-mouse-cd45.612924
Pacific Blue Rat anti-Mouse CD3	BioLegend	155612	0.25 μg/test	https://www.biolegend.com/en-us/products/pacific-blue-anti-mouse-cd3e-antibody-16478?GroupID=BLG4744
PE Rat anti-Mouse F480	BioLegend	123109	0.5 μg/test	https://www.biolegend.com/en-us/products/pe-anti-mouse-f4-80-antibody-4068?GroupID=BLG5319
PE Cyanine7 Rat anti-Mouse CD4	BioLegend	100422	0.25 μg/test	https://www.biolegend.com/en-us/products/pe-cyanine7-anti-mouse-cd4-antibody-1919?GroupID=BLG4211
PerCP-Cy5.5 Rat anti-Mouse CD8	BioLegend	100734	0.5 μg/test	https://www.biolegend.com/en-us/products/percp-cyanine5-5-anti-mouse-cd8a-antibody-4255?GroupID=BLG2559
FITC Rat anti-Mouse IFNγ	eBioscience	11-7311-82	0.5 μg/test	https://www.thermofisher.cn/cn/en/antibody/product/IFN-gamma-Antibody-clone-XMG1-2-Monoclonal/11-7311-82
PE Rat anti-Mouse IL4	eBioscience	12-7041-82	0.125 μg/test	https://www.thermofisher.cn/cn/en/antibody/product/IL-4-Antibody-clone-11B11-Monoclonal/12-7041-82
APC Rat anti-Mouse IL9	BioLegend	514106	0.125 μg/test	https://www.biolegend.com/en-us/search-results/apc-anti-mouse-il-9-antibody-5980
FITC Rat anti-Mouse IL17	BioLegend	506908	0.25 μg/test	https://www.biolegend.com/en-gb/products/fitc-anti-mouse-il-17a-antibody-3534?GroupID=GROUP24
Alexa Fluor 488 Rat anti-Mouse FoxP3	eBioscience	53-5773-82	0.25 μg/test	https://www.thermofisher.cn/cn/en/antibody/product/FOXP3-Antibody-clone-FJK-16s-Monoclonal/53-5773-82

DNA/cDNA Clones

Clone Name	Sequence	Source / Repository	Persistent ID / URL

Cultured Cells

Name	Vendor or Source	Sex (F, M, or unknown)	Persistent ID / URL
Primary aortic fibroblasts	Primary cells	M	
Primary T cells	Primary cells isolated from spleen of WT/TKO mice	M	
HEK293T cells	CRL-3216, ATCC	Unknown	https://www.atcc.org/products/crl-3216

Data & Code Availability

Description	Source / Repository	Persistent ID / URL
Single cell RNA sequencing	GEO datasets	
Bulk RNA sequencing	GEO datasets	

Other

Description	Source / Repository	Persistent ID / URL
Angiotensin II	A9525, Sigma-Aldrich	https://www.sigmaaldrich.cn/CN/en/product/sigma/a9525
Osmotic mini pumps	Model 2004 and 2006, ALZET	https://www.alzet.com/products/alzet_pumps/
Recombinant mouse IL-9	409-ML, R&D System	https://www.rndsystems.com/products/recombinant-mouse-il-9-protein_409-ml
Mouse T-Activator CD3/ CD28 for T-Cell expansion and activation	11452D, Gibco	https://www.thermofisher.com/order/catalog/product/11452D
Mouse Albumin ELISA Kit	ab207620, Abcam	https://www.abcam.com/mouse-albumin-elisa-kit-ab207620.html
Creatinine Assay Kit	ab65340, Abcam	https://www.abcam.com/creatinine-assay-kit-ab65340.html
Mouse KIM-1 ELISA Kit (KIM1)	ab213477, Abcam,	https://www.abcam.com/mouse-tim-1-elisa-kit-kim-1-ab213477.html
Von Kossa Stain Kit (Calcium Stain)	ab150687, Abcam	https://www.abcam.com/von-kossa-stain-kit-calcium-stain-ab150687.html
Alexa Fluor TM 488 conjugated wheat germ agglutinin (WGA)	W11261, Invitrogen	https://www.thermofisher.cn/order/catalog/product/W11261
PMA	P1585, Sigma	https://www.sigmaaldrich.cn/CN/en/product/sigma/p1585
ionomycin	I0634, Sigma Aldrich	https://www.sigmaaldrich.cn/CN/en/product/sigma/i0634
Brefeldin A	B5936, Sigma Aldrich	https://www.sigmaaldrich.cn/CN/en/product/sigma/b5936
Cytofix/Cytoperm kit	554714 BD, Biosciences	https://www.bdbiosciences.com/en-us/products/reagents/flow-cytometry-reagents/research-reagents/buffers-and-supporting-reagents-ruo/bd-cytofix-cytoperm-fixation-permeablization-kit.554714
Mouse CD4+ T Cell Isolation Kit	130-104-454, Miltenyi Biotec,	https://www.miltenyibiotec.com/JP-en/products/cd4-t-cell-isolation-kit-mouse.html?countryRedirected=1
Mouse CD3IFNɛ MicroBead Kit	130-094-973, Miltenyi Biotec,	https://www.miltenyibiotec.com/JP-en/products/cd3e-microbead-kit-mouse.html?countryRedirected=1#gref
CD45-Microbeads Kit	130-052-301, Miltenyi Biotec,	https://www.miltenyibiotec.com/JP-en/products/cd45-microbeads-mouse.html?countryRedirected=1#gref
anti-PE Microbeads	130-048-801, Miltenyi Biotec	https://www.miltenyibiotec.com/JP-en/products/anti-pemicrobeads.html?countryRedirected=1#gref
Lipofectamine 2000	11668019, Invitrogen	https://www.thermofisher.cn/order/catalog/product/11668019
Il9 promoter reporter	GeneCopoeia (MPRM39766-PG04; NM_008373)	https://www.genecopoeia.com/product/search/detail.php?prt=22&cid=&key=MPRM39766&type=promoter&choose=IL9
HDAC1 siRNA	s119558, Thermofisher	https://www.thermofisher.cn/order/genome-database/details/sirna/s119558?CID=&ICID=&subtype=
Non-specific siRNA	4390843, Thermofisher,	https://www.thermofisher.cn/order/catalog/product/4390843
Secrete-Pair Dual Luminescence Assay	LF032, GeneCopoeia	https://www.genecopoeia.com/product/secrete-pair/dual-luminescence-assay/

Other		
Description	**Source / Repository**	**Persistent ID / URL**
Chromatin Immunoprecipitation (ChIP) assay kit	#9003, Cell signal	https://www.cellsignal.com/products/chip-kits-reagents/enzymatic-chromatin-ip-kit-magnetic-beads/9003
SYBR Green Master Mix	GoTag PCR system, Promega M7122	https://www.promega.com.cn/products/pcr/taq-polymerase/gotaq-master-mixes/
Pierce™ Protein G Magnetic Beads	88847, Thermo Scientific	https://www.thermofisher.cn/order/catalog/product/88847
Fluo-8 No Wash Calcium Assay kit	ab112129, Abcam,	https://www.abcam.com/fluo-8-calcium-fluxassay-kit-no-wash-ab112129.html